Fast Impedance Simulation of Lithium-Ion Batteries with Pseudo-Two Dimensional Electrochemical Models

Manan Pathak,[1,*] Matthew D. Murbach,[1,*] Chintan Pathak,[1] Tae-Jin Jang,[1,*] Yanbo Qi,[1,*] Daniel T. Schwartz,[1,] and Venkat R. Subramanian[1,2,***,z]**

[1] *Department of Chemical Engineering, University of Washington, Seattle, Washington 98195, USA*
[2] *Pacific Northwest National Laboratory, Richland, Washington 99352, USA*

A hybrid analytical-collocation approach for fast simulation of the impedance response for a Li-ion battery using the pseudo-two dimensional model is presented. The impedance response of the spherical diffusion equations is solved analytically and collocation is performed on the resulting boundary value problem across the electrode and separator thickness using an orthogonal collocation scheme based on Gauss-Legendre points. The profiles for a frequency range from 0.5 *mHz* to 10 *kHz* are compared with the numerical solution obtained by solving the original model in COMSOL Multiphysics. The internal variable profiles across a wide range of frequencies are compared between the two methods and the accuracy, robustness, and computational superiority of the proposed hybrid analytical-collocation approach is presented. The limitations of the proposed approach are also discussed. A freeware for academic use that reads the various battery parameters and frequencies of interest as input, and predicts the battery impedance for a half cell and full cell, is also developed and a means to access it is reported in this paper.

 [DOI: 10.1149/2.0831805jes]

Manuscript submitted October 30, 2017; revised manuscript received March 12, 2018. Published May 3, 2018.

Electrochemical impedance spectroscopy (EIS) has been widely used to study the linear dynamics of many electrochemical systems, including Li-ion batteries.[1–4] Most physical and chemical processes in an electrochemical system possess distinct characteristic time constants, enabling EIS to distinguish these processes by their frequency response. The dynamics of the porous electrodes used inside most commercially available Li-ion batteries are governed by the conduction and mass transfer in the solid and the electrolyte phase, and electro-chemical kinetics at the solid-electrolyte interface. Because EIS is able to separate processes by their time-scales, it is often possible to see changes in each battery electrode as well as the degradation that leads to capacity fade of the batteries.[5–8]

Equivalent circuits are the most commonly used models to study the impedance response of batteries; however, the use of networks of circuit elements can suffer from a lack of physical interpretability and model degeneracy.[9] Though much less used, physics-based models can provide more direct insight into the impedance response of a battery. A critical review describing various continuum and multiscale physics-based models has been published before.[10] Mathematically, physics-based impedance models are transformed from the time-domain to the frequency-domain by assuming a steady-periodic response, thereby eliminating time as an independent variable.[11] Analytical solutions for similar systems with a limited set of physics have been reported since 1989 (Equation 53),[12] but due to the difficulty in separating the real and imaginary parts in parametric form, the analytical solution needs to be derived repeatedly for different parameter sets, making it less efficient. Most rigorous physics-based models for the impedance of a Li-ion battery employ a numerical scheme to solve the resulting equations.[11,13,14] The resulting equations are computationally expensive to solve, and this reduces their usefulness for multi-parameter optimization and analysis of different mechanisms from experimental impedance data.

Part of the computational complexity in solving these models arises from the coupling between mass transfer, kinetics, and thermodynamics across the thickness of the electrode to the solid phase diffusion inside the solid particles. Simultaneous simulation of multiple coupled linear equations is inherently related to exponential matrix, introduced by N. R. Amundson to the chemical engineering field.[15] In addition to the initial value problems, an unified approach to solve coupled boundary value problems (BVPs) has also been explored.[16] This approach is effective even for elliptic partial differential equations (PDEs) in which more than 100 coupled BVPs were integrated analytically.[17]

Though never explored with frequency-domain physics-based model formulations, there have been significant advances to accelerate time-domain computations of discharge-charge curves using physics-based battery models.[18–23] One strategy for reducing the simulation time has been approximating solid phase diffusion using various polynomial approximations.[24–27] Approximations were typically applied that reduced the number of state variables, along with the computational time. While Duhamel's superposition method reduces the number of state variables (for example, it removes the radial coordinate '*r*' from the model simulation), it is not ideal for reducing the computational time, as adaptive solvers for integrating the discretized system of differential algebraic equations (DAEs) ($\frac{dy}{dt} = f(y, z), 0 = g(y, z)$) cannot be used. Even though we have applied polynomial approximations for concentration in the solid phase for our past work,[24] these approximations are not needed for AC impedance simulation as the radial dependence can be removed by solving analytically for the solid phase impedance response.

Closed-form analytical solutions of the impedance have been derived for certain cases, but these are only valid under specific design considerations or limited operating conditions. For example, an analytical solution for the impedance response of porous intercalation electrodes in the absence of solid-phase diffusion limitations has been presented.[28] Similarly, analytical solutions have been derived for estimating physical properties of non-insertion porous electrodes in symmetric cells, and of electrodes without electrolyte-phase diffusion limitations.[29,30] Symbolic closed-form solutions have also been developed for predicting the impedance response in planar electrodes, due to diffusion process.[31] Moreover, a general analytical expression for the impedance response for Li-ion cells, accounting for the reaction kinetics at the interface, along with potential distribution and mass transport in the solid and electrolyte phase has also been proposed.[32–34] However, most of these methods do not account for the entire battery physics, and others numerically fail for high frequencies, unless very high numbers of polynomial coefficient terms are used. Also, using the analytical solution requires operation in complex domain and separating the real and imaginary parts of impedance in parametric form is challenging, which limits its use for real-time simulation and estimation.

*Electrochemical Society Student Member.
**Electrochemical Society Fellow.
***Electrochemical Society Member.
[z]E-mail: vsubram@uw.edu

In this paper, we propose a computationally efficient way to solve the impedance equations for the pseudo-2 dimensional (P2D) model by first applying a coordinate transformation, then orthogonal collocation to represent the model equations. After applying a time periodic solution form,[11] the governing equations for the original P2D model are converted to partial differential equations in the frequency domain, where the independent variables are x (transverse spatial coordinate across the cell), and r (local radial coordinate for the spherical electrode particles). The radial dependence of the solid phase concentrations can be solved analytically, even for the cases in which solid phase diffusion coefficient is dependent on the concentration inside the solid particle, as only the linear terms are considered for the linear AC impedance models. Once the analytical solution is available, the dependency in radial coordinate 'r' is removed and the model just becomes a BVP in the spatial coordinate 'x', with corresponding boundary conditions for each variable. Solutions to the dependent variables such as the complex oscillating concentrations and potentials in the system are parameterized in frequency domain, along with the physicochemical and geometric properties and electrodes, electrolyte, and cell configuration. The details for obtaining the analytical solution for the solid-phase concentration equations, are given in the appendix. The resulting equations can be solved using finite difference method, or using finite element method, in a computational platform such as COMSOL Multiphysics.[35]

To simplify the computation of the BVPs, we apply a coordinate transformation, to rescale the spatial coordinate, as described in more detail below.

Coordinate Transformation

A Li-ion battery consists of cathode, separator and anode. The model equations must be solved in each region simultaneously, with the boundary conditions at the interfaces coupling the variables in each region. As proposed earlier by Northrop et al., to reduce the required computation, each region is rescaled to be solved within a spatial domain from $X = [0, 1]$.[23] The spatial coordinate is rescaled as:

$$X = \frac{x}{l_p}, 0 \le x \le l_p \quad [1]$$

$$X = \frac{x - l_p}{l_s}, l_p \le x \le l_p + l_s \quad [2]$$

$$X = \frac{x - l_p - l_s}{l_n}, l_p + l_s \le x \le l_p + l_s + l_n \quad [3]$$

The resulting transformed governing equations for the model along with boundary conditions, are given in Table AI in the appendix.

Applying Orthogonal Collocation

The theory behind orthogonal collocation has been extensively developed, and the stability has been studied.[36–38] In order to solve the equations, a certain number of node points are chosen in each region. The variables to be solved in each region, are assumed to be represented by a polynomial function,

$$u_k(X) = \sum_{i=0}^{N+1} f_i^k X^i = f_0^k + f_1^k X + f_2^k X^2 + ... + f_N^k X^N + f_{N+1}^k X^{N+1} \quad [4]$$

where u_k represents the variable to be solved, f_i^k represents the coefficient of X^i, and the superscript 'k' represents the particular region where the equation is solved (p, s, n for the positive electrode, separator, and negative electrode respectively).

The governing equations of the model are then solved at the internal node points, whereas the boundary conditions govern the dynamics at the boundary points. The node points are chosen as the roots of the N^{th} order Jacobi polynomial. We describe the process of collocation for $N = 1$ internal node point in each region in appendix. For illustration purposes, arbitrary constants are used for approximating all variables using a polynomial profile. An alternate Lagrangian polynomial form offers the ability to write the polynomial representation for a variable by simply using the dependent variable at the internal collocation points and the boundary points. For example, for $N = 1$, a polynomial for a variable V, can be written using V_0, V_1 and V_2 as

$$V(X) = \frac{V_0(X - 0.5)(X - 1)}{(0 - 0.5)(0 - 1)} + \frac{V_1(X - 0)(X - 1)}{(0.5 - 0)(0.5 - 1)} + \frac{V_2(X - 0)(X - 0.5)}{(1 - 0)(1 - 0.5)}$$

where V_0, V_1 and V_2 are the variables at $X = 0$, $X = 0.5$ (first and only collocation point) and $X = 1$.

It should be noted that after applying orthogonal collocation, the resulting equations are linear equations in the unknown variables and can be solved using any linear solver. This approach can easily be extended to higher number of collocation points until convergence is achieved. As discussed later, higher frequencies necessitate a larger number of collocation points.

Results

The parameter values used for this work are listed in Table AIII in the appendix. The resulting set of equations from the collocation approach is solved in the *Maple* 17 classic worksheet environment and is solved for a range of 70 different frequencies, ranging from 0.5 *mHz* to 10 *kHz* and were also independently solved in C. The results were independently compared with ones obtained by solving the governing equations in COMSOL 4.4, which uses finite element method for the simulation.[35] While solving in COMSOL, a physics-controlled '*extremely fine*' mesh was selected in both the radial and the spatial direction, and the equations were solved using the *MUMPS* solver with a relative tolerance of 1e-4, to ensure convergence. The total computational time required to solve the equations on an Intel(R) Xeon(R) E5-2687 W 0 @ 3.1 *GHz* CPU with a 32 GB RAM for $N = 17$ internal collocation node points was about 4.3 seconds in *Maple* 17, as opposed to over 8 minutes required to solve in COMSOL for the same set of frequencies. The memory required for *Maple* 17 was about 180 MB, as opposed to COMSOL which required in excess of 2 GB. The computational time is even faster when moved to a C-based environment (a freeware is available on our website).

Figure 1 shows the Nyquist plot, plotting the imaginary component versus the real component of the linear impedance, for a range of frequencies, obtained for $N = 17$ internal collocation node points.

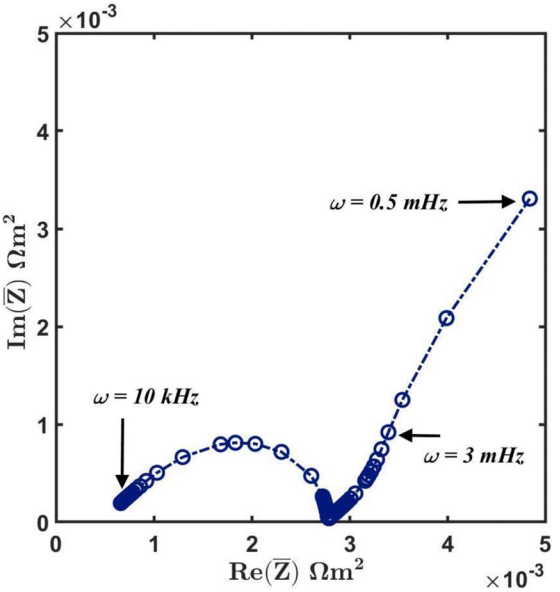

Figure 1. Nyquist plot of the imaginary part of impedance vs the real part of impedance.

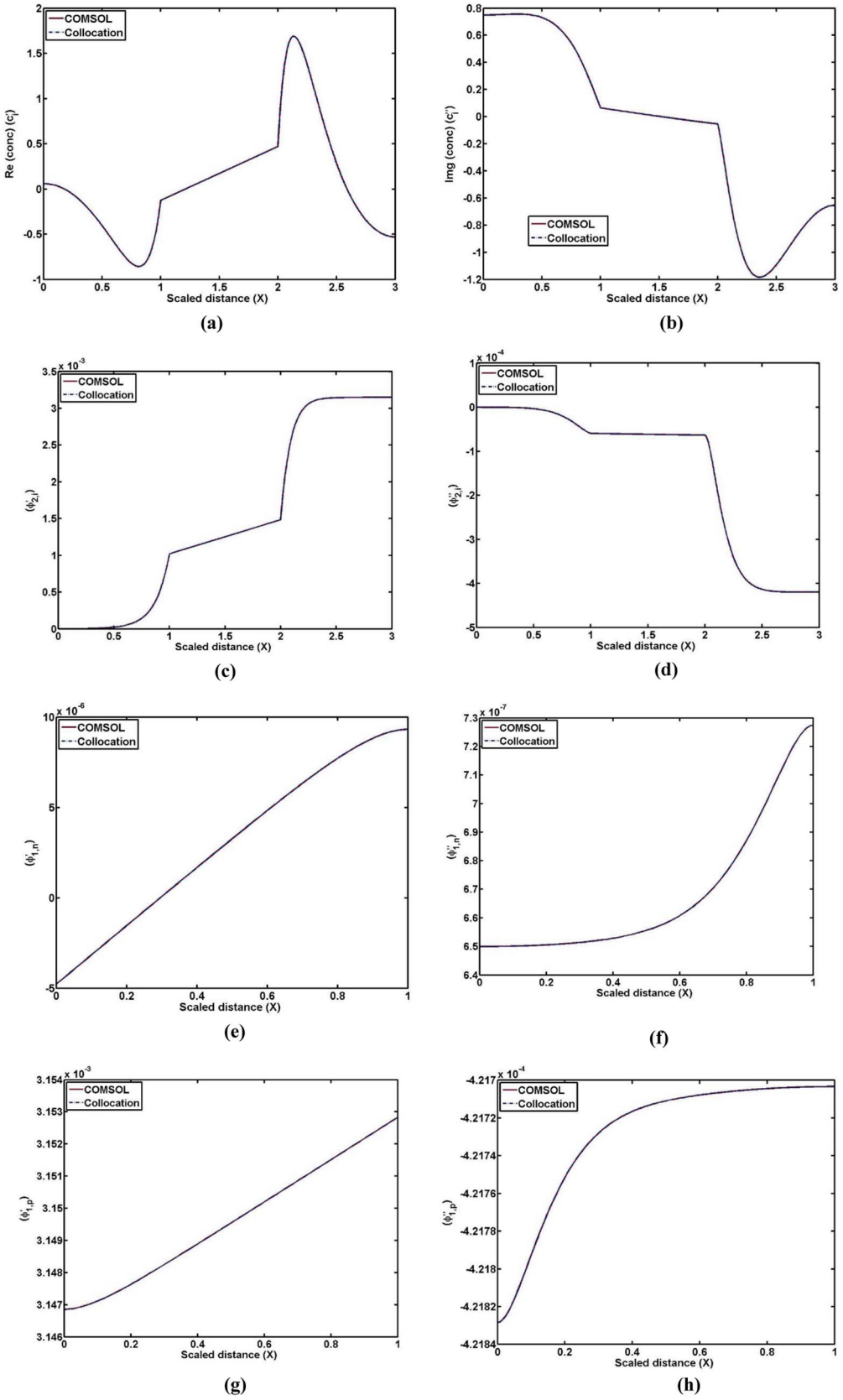

Figure 2. Comparison of variation of internal variables with scaled distance (X) for orthogonal collocation and COMSOL for $\omega = 10\ mHz$ for (a) Real part of concentration (c'_i) (b) Imaginary part of concentration (c''_i) (c) Real part of liquid phase potential ($\Phi'_{2,i}$) (d) Imaginary part of liquid phase potential ($\Phi''_{2,i}$) (e) Real part of solid phase potential in the negative electrode ($\Phi'_{1,n}$) (f) Imaginary part of solid phase potential in the negative electrode ($\Phi''_{1,n}$) (g) Real part of solid phase potential in the positive electrode ($\Phi'_{1,p}$) (h) Imaginary part of solid phase potential in the positive electrode ($\Phi''_{1,p}$).

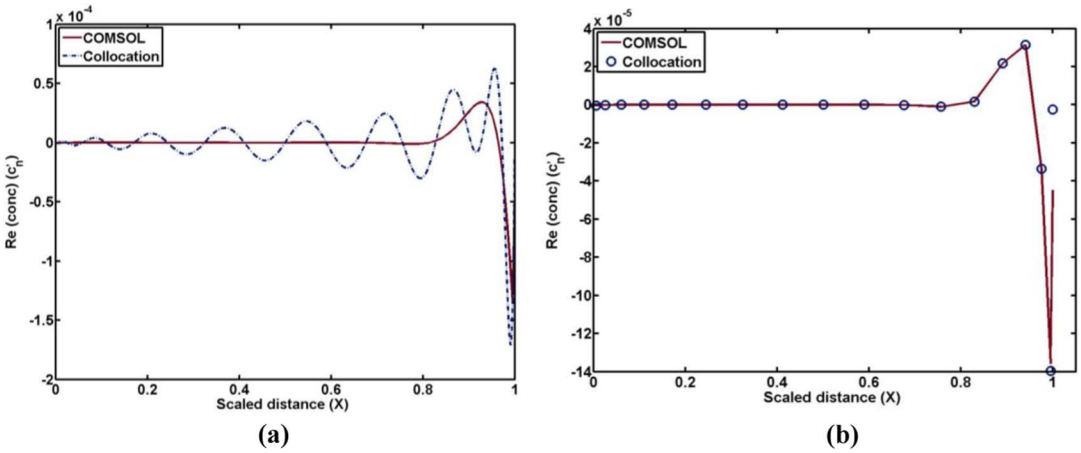

Figure 3. Comparison of Real part of concentration vs x in the negative electrode for $\omega = 3000\ Hz$ (a) plotted for the continuous polynomial solution (b) plotted only at discrete collocation points.

The plot shows the qualitative experimental response observed for Li-ion batteries, with the mass transfer effects (in the solid phase) governing the dynamics at low frequencies, and the interfacial and kinetic effects governing the response at medium frequencies, before a purely ohmic response at very high frequencies.

Figures 2a–2h represents the comparison of spatial variation of various variables vs X (thickness of the battery), in each region from the current collector at the negative electrode ($X = 0$) to the current collector at the positive electrode ($X = 3$), for COMSOL, and the results obtained using for the collocation approach at a frequency of 10 *mHz*. The profiles match exactly.

At high frequencies, oscillations are observed in the collocation solution. Figure 3a shows the comparison of the variation of the real part of concentration vs X in the negative electrode at a frequency of 3000 *Hz*, obtained in COMSOL, and collocation using $N = 17$ internal node points. Due to high frequency, extremely steep gradients are developed near the anode-separator interface, and the separator-cathode interface, resulting in a significant boundary layer. To capture this phenomenon effectively, a very high number of collocation points are needed to exactly match the continuous profile in the spatial direction. However, the accuracy of the solution is maintained at the collocation node points, without any oscillations. Figure 3b shows the comparison of the values of the real part of concentration in the negative electrode obtained in COMSOL, and obtained through collocation, plotted only at the discrete collocation points. At points away from the interface, the solution matches well. However, the error is slightly higher close to the boundary at the interface, which needs even larger collocation points.

While using a continuous solution in the spatial coordinate 'x' (independent variable) in applying orthogonal collocation, accuracy and stability are guaranteed only at the collocation points, and a linear interpolation between two collocation points will give a more stable solution, compared to the continuous polynomial solution, which might oscillate at high frequencies. Use of alternate collocation approaches such as Chebyshev collocation, reduces the oscillations for the continuous polynomial solution (i.e., continuous polynomial as in Equation 4), however the resulting accuracy at the collocation points is lower. The accuracy is highest for Gauss collocation, for rectangular coordinates.[39] Accuracy at the boundary points can be increased by using a higher number of collocation points throughout the region, or by using orthogonal collocation on finite elements (OCFE). OCFE involves dividing the entire spatial domain into smaller finite elements and applying orthogonal collocation in each finite element. The number of collocation points can be varied in each element, based on the physics of the particular problem. For example, for this problem, higher collocation points can be chosen in elements closer to the interfaces, as compared to the current collectors, since the gradients are steeper closer to the interface. However, the proposed collocation approach already guarantees the desired accuracy in linear impedance (as the accuracy is higher closer to the current collector), and hence other collocation approaches are not explored in this work.

Figures 4a, 4b shows the real part of the concentration in the solid phase in the negative and positive electrode respectively, vs the radial coordinate r at a frequency of 10 *mHz*, at $X = \{0, 0.5, 1\}$. The concentration gradient is higher closer to the interface than, near the current-collector. Figures 5a, 5b shows the real part of the concentration in

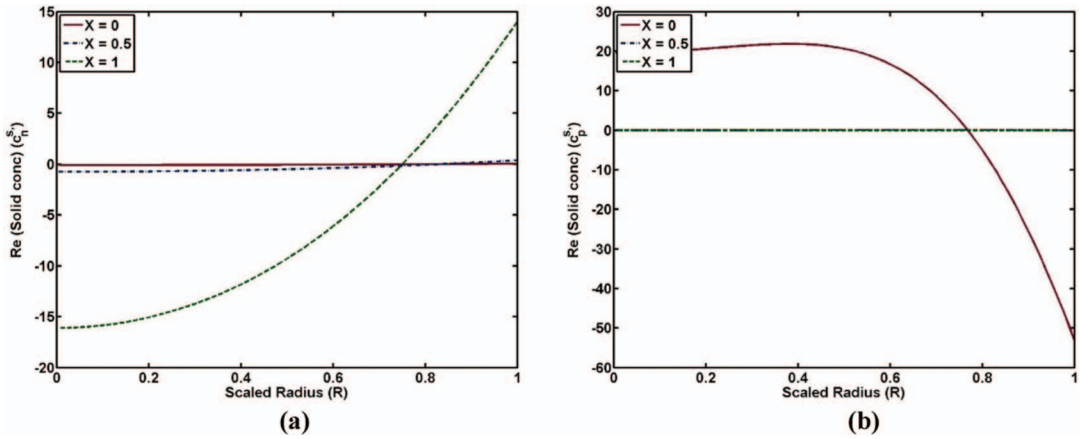

Figure 4. Plot of real part of the solid phase concentration in the (a) negative and (b) positive electrode vs scaled radius (R) at $X = 0, 0.5\ and\ 1$ for $\omega = 10\ mHz$.

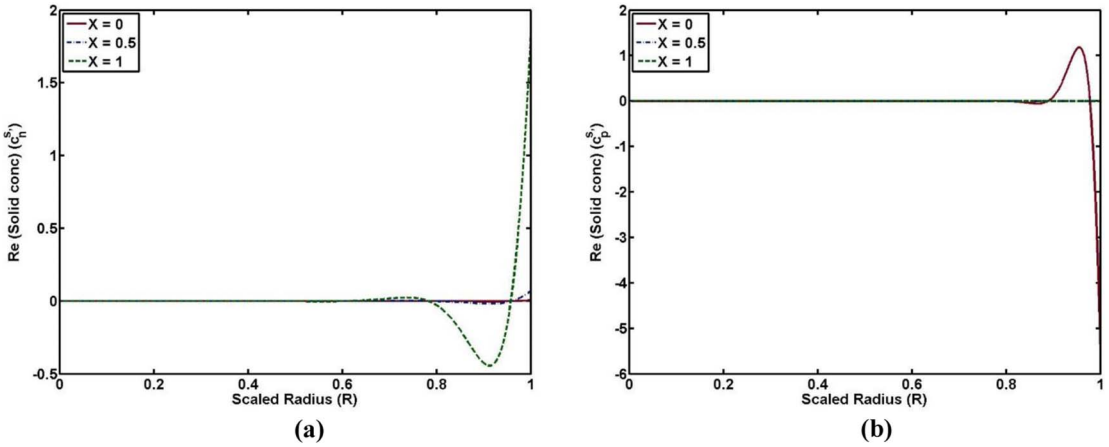

Figure 5. Plot of (a) Real part of solid phase concentration in the negative and (b) Real part of solid phase concentration in the positive electrode vs scaled radius (R) at $X = 0, 0.5$ *and* 1 for $\omega = 1$ *Hz*.

the solid phase in the negative and positive electrode respectively, vs the radial coordinate r at a frequency of 1 *Hz*, at $X = \{0, 0.5, 1\}$. As the frequency increases, very steep gradients are developed closer to the surface of the particle.

This approach of orthogonal collocation can easily be extended for higher order terms in the polynomial representation, which are needed for higher frequencies. Figure 6 shows the plot for number of node points required for various frequencies, for 6-digit accuracy, when compared to the COMSOL solution. As discussed above, the required number of points increase with increasing frequency as expected.

Table I shows the values of the real and imaginary part of impedance up to 7 decimal digits obtained after choosing N = 3, 7, 15 and *17* internal node points along with values obtained in COMSOL at specific frequencies. A frequency of 10 *mHz* requires $N = 7$ internal node points, to match with the values obtained in COMSOL for 6-digits accuracy. As mentioned above, the required number of node points increase with increasing frequency with $N = 15$ internal node points required for high frequency of 3000 *Hz*. The table also shows values obtained for internal node points $N = 17$, which match with the values obtained for $N = 15$, up to 6 digits, that proves the self-convergence and consistency of the approach. Typically, COMSOL uses a weak form of the original set of PDEs, but in the collocation approach, the original form (strong form) of the model is simulated. Because of the linearity of the impedance equations in this case, collocation in the spatial dimension 'x' gives good accuracy. It is possible to apply spectral methods in weak form as well, but the application of that is beyond the scope of this paper.

It is important to note that the number of node points needed for the desired accuracy also depends on the set of parameters being used for the system, as the classification of low/high frequency is determined entirely by the time constants of various physical processes, which are dictated by the geometric and physicochemical parameters of the battery. For example, the time constant of the electrode for the kinetic processes depend on the charge transfer resistance and the double layer capacitance of the electrode. To illustrate this, Figure 7 shows the Nyquist plot comparison for different values of the double layer capacitance for the anode. The distinction in the two arcs of the individual electrodes gets more pronounced as the capacitance of the double layer increases. Table II shows the comparison between the real and imaginary part of linear impedance values for different values of the double layer capacitance of anode, for $N = 15$ and $N = 17$. While the solution matches until 6 decimal digits for $Cdl_n = 10$, it only matches until 5 decimal digits for $Cdl_n = 100$ and $Cdl_n = 1000$. This shows that even higher points than 17 might be required to get convergence for such high values of the anode double layer capacitance, for the same characteristic frequency of 3000 *Hz*. Similar analysis can be done for other sets of parameter values. Since the analysis in this work is only done for one set of parameter values,

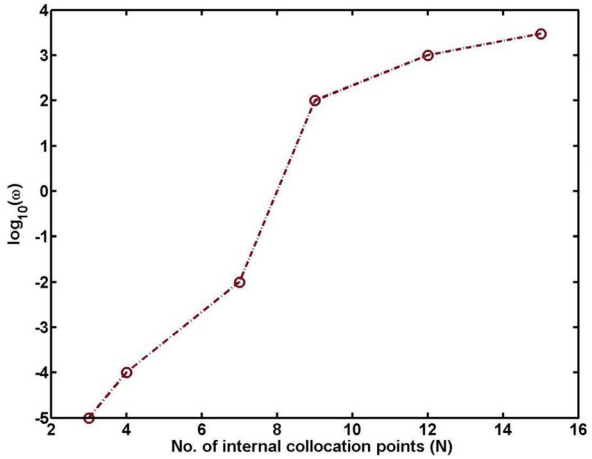

Figure 6. Plot of $\log_{10}(\omega)$ vs Number of internal collocation points (N) required for 6-digits accuracy.

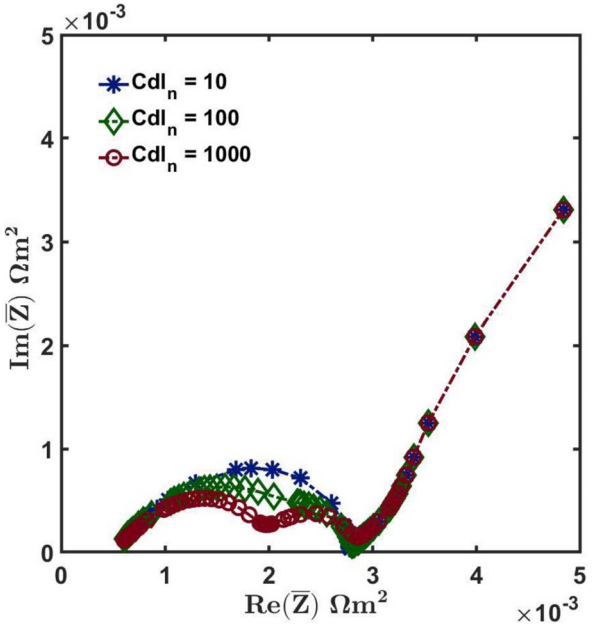

Figure 7. Nyquist plot for linear impedance for $Cdl_n = 10, 100$ *and* $1000\,\mu F/cm^2$.

Table I. Values of Real and Imaginary part of impedance for various number of collocation points along with COMSOL values.

	$N = 3$		$N = 7$		$N = 15$		$N = 17$		COMSOL	
Frequency (ω) (Hz)	$\mathrm{Re}(\bar{Z})$ (Ωm^2)	$\mathrm{Im}\, g(\bar{Z})$ (Ωm^2)	$\mathrm{Re}(\bar{Z})$ (Ωm^2)	$\mathrm{Im}\, g(\bar{Z})$ (Ωm^2)	$\mathrm{Re}(\bar{Z})$ (Ωm^2)	$\mathrm{Im}\, g(\bar{Z})$ (Ωm^2)	$\mathrm{Re}(\bar{Z})$ (Ωm^2)	$\mathrm{Im}\, g(\bar{Z})$ (Ωm^2)	$\mathrm{Re}(\bar{Z})$ (Ωm^2)	$\mathrm{Im}\, g(\bar{Z})$ (Ωm^2)
0.01	0.0036412	0.0003119	0.0031576	0.00422005	0.0031576	0.0004223	0.0031576	0.0004223	0.0031576	0.0004223
0.1	0.0034421	0.0001167	0.0028985	0.0001365	0.0028978	0.0001369	0.0028978	0.0001369	0.0028978	0.0001369
1	0.0033643	0.0000331	0.0028029	0.0000475	0.0028013	0.0000475	0.0028013	0.0000475	0.0028013	0.0000475
10	0.0033468	0.0000449	0.0027737	0.0000655	0.0027727	0.0000656	0.0027727	0.0000656	0.0027727	0.0000656
100	0.0032124	0.0003164	0.0026064	0.0004714	0.0026058	0.0004728	0.0026058	0.0004728	0.0026058	0.0004728
1000	0.0024953	0.0002098	0.0012766	0.00061305	0.0012916	0.0006642	0.0012916	0.0006642	0.0012916	0.0006642
3000	0.0024487	0.0000739	0.0009827	0.0002832	0.0009198	0.0004208	0.0009195	0.0004205	0.0009195	0.0004206

Figure 6 shows the requirement of the number of collocation points in a qualitative sense.

In this work, the same number of collocation points were used in each region, namely cathode, separator and anode. However, depending on the problem, different number of collocation points can be used in different regions to get the desired accuracy. As there is no solid-phase in the separator, a lower number of collocation points in that region could still ensure an overall 6-digits accuracy of linear impedance. This kind of variable collocation approach will reduce the resulting number of equations to be solved, which will in turn make the algorithm even faster. In this way, a robust, fail-proof and fast solving code for calculating linear impedance for a full cell has been obtained that can be used for various goals, including parameter estimation for physics-based models using the EIS data.

Half Cell Impedance Simulation

In order to improve the performance of lithium-ion batteries, a lot of efforts have been devoted to the development of materials for each component in the battery system. When testing new cathode or anode material, a half-cell configuration with the new material being one electrode and lithium metal being the counter electrode is commonly used by material scientists.[40,41] To broaden the range of application of the proposed impedance simulation approach and to meet the demand of analyzing half-cell impedance data, simulation of the impedance for such a half-cell system is also reported here. Cathode-lithium half-cell is used as an example, but anode-lithium half-cell system can also be simulated using the same approach.

The governing equations for the separator and the cathode in the half cell are the same as in the full cell. The interface between the separator and the anode now becomes the interface between the separator and the lithium metal, which is active in electrochemical reactions. For the Lithium-separator boundary, Butler-Volmer kinetic expression is assumed and determines the potential drop across the interface.[42] The equations and modified boundary conditions are listed in Table AIV in the appendix for clarity. This half-cell model can also be viewed as a base model for fresh lithium metal batteries before cycling.

A Nyquist plot for a half cell using $N = 17$ collocation node points with the parameters listed in Table AIII is shown in Figure 8. Compared with the full-cell impedance curve, the half-cell impedance curve has the same shape with an overall reduced value, as expected.

Table II. Values of Real and Imaginary part of impedance for different anode double layer capacitance (Cdl_n) for various number of collocation points for a frequency of 3000 *Hz*.

	$N = 15$		$N = 17$	
Cdl_n $\left(\frac{\mu F}{cm^2}\right)$	$\mathrm{Re}(\bar{Z})$ (Ωm^2)	$\mathrm{Im}\, g(\bar{Z})$ (Ωm^2)	$\mathrm{Re}(\bar{Z})$ (Ωm^2)	$\mathrm{Im}\, g(\bar{Z})$ (Ωm^2)
10	0.0009198	0.0004208	0.0009195	0.0004205
100	0.0007877	0.0003025	0.0007898	0.0003049
1000	0.0007672	0.00002546	0.0007602	0.0002561

The ohmic resistance decreases slightly when removing the graphite electrode while the reduction in charge-transfer resistance is more noticeable.

To test the robustness of this approach, a different set of parameters were used in the half-cell impedance simulation to represent a different chemistry with a different cell design. The new set of parameters are listed in Table AV.[43] The impedance of the new half-cell (half cell #2) compared to the half-cell with parameters in Table AIII (half cell #1) is plotted in Figure 9. The proposed hybrid analytical-collocation approach is very stable over the physically reasonable range of the parameter values. The difference in chemistry and cell design can be well captured by this impedance model and is reflected in the Nyquist plot.

Code dissemination.—An executable freeware code for both full-cell and half-cell simulations is hosted on the corresponding author's website at *http://depts.washington.edu/maple/EIS.html* that can be downloaded to calculate the linear impedance for given frequency with $N = 21$ and $N = 23$ internal node points to check for self-convergence, and gives the real and imaginary part of impedance. The parameters and frequency are read from an external text file. The instructions for running the code are also given on the website. These codes are provided without any restrictions for academic use and not for commercial use. More details about using the codes are provided at the website. Current implementation in C (converted to exe codes) is not the final optimized version, and CPU time and memory requirements are expected to be even better when we continue to optimize the algorithms.

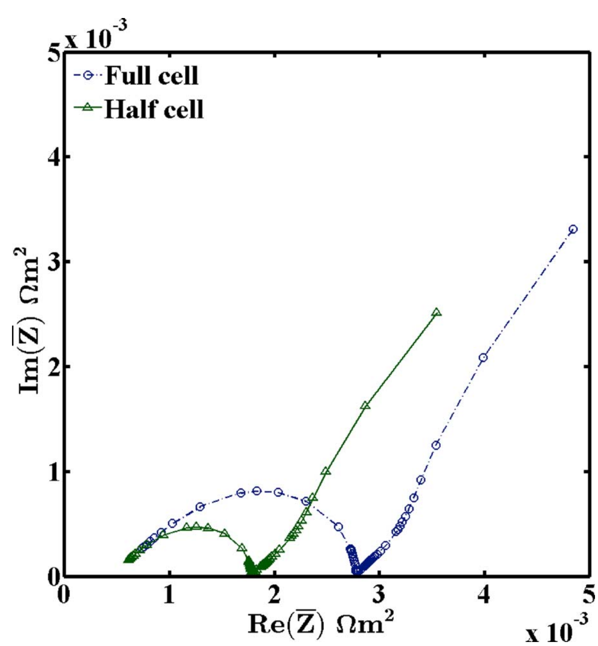

Figure 8. Nyquist plot for linear impedance of a full cell and a half cell.

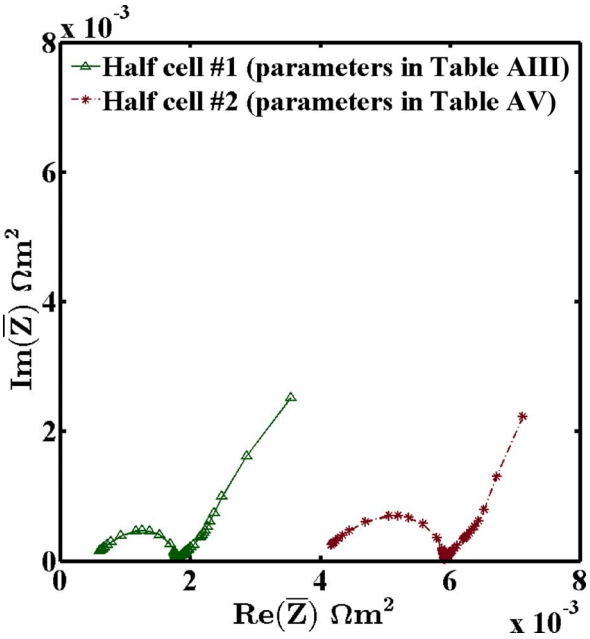

Figure 9. Nyquist plot for linear impedance of half cell #1 with parameters from Table AIII, and half cell #2 with parameters from Table AV to demonstrate the hybrid approach's robustness in handling different chemistries and designs.

Conclusions

A hybrid method of orthogonal collocation across the electrodes coupled with the analytical solution in the solid-phase, for solving the impedance equations for the P2D models that is extremely fast, robust and fail-proof, is presented. Such a model can be used for parameter estimation based on experimental data in real-time, i.e. the impedance equipment can display P2D model predictions before the experiment is completed. Future work involves adding more physics such as the SEI layer dynamics to the existing model, extending the technique to second and higher order harmonics, and estimating the material, transport and kinetic properties using the first and second harmonics signals, which could lead to more insight into battery dynamics that is not captured by EIS.

Acknowledgments

The authors thank the Department of Energy (DOE) for providing partial financial support for this work, through the Advanced Research Projects Agency (ARPA-E) award number DE-AR0000275, along with the Assistant Secretary for Energy Efficiency and Renewable Energy, Office of Vehicle Technologies of the DOE through the Advanced Battery Material Research (BMR) Program (Battery500 consortium). The authors would also like to thank the Clean Energy Institute (CEI) at the University of Washington (UW) and the Washington Research Foundation (WRF) for their monetary support during this work.

Appendix

Example for N = 1 collocation point.—*Equations in the negative electrode.—* Consider the governing equations from Table AI, for the real and imaginary parts of the electrolyte concentration, potential in the solid-phase, and potential in the liquid-phase, in the negative electrode along with the boundary conditions. The expressions for the current densities and the overpotentials are substituted from Table AII.

$$-\varepsilon_n c''_n\omega = \frac{1}{l_n}\frac{\partial}{\partial X}\left[\frac{D_{\text{eff,n}}}{l_n}\frac{\partial c'_n}{\partial X}\right] + a_n(1-t_+)\left(\frac{i0_n(\alpha_A+\alpha_C)}{RT}\left(\Phi'_{1,n}-\Phi'_{2,n}\right.\right.$$
$$\left.\left.-dUdC_n * cns'\right) - \frac{\omega Cdl_n}{F}\left(\Phi''_{1,n}-\Phi''_{2,n}\right)\right) \quad [A1]$$

$$\varepsilon_n c'_n\omega = \frac{1}{l_n}\frac{\partial}{\partial X}\left[\frac{D_{\text{eff,n}}}{l_n}\frac{\partial c''_n}{\partial X}\right] + a_n(1-t_+)\left(\frac{i0_n(\alpha_A+\alpha_C)}{RT}\right.$$
$$\left(\Phi''_{1,n}-\Phi''_{2,n}-dUdC_n * cns''\right) + \frac{\omega Cdl_n}{F}\left(\Phi'_{1,n}-\Phi'_{2,n}\right)\Big)$$
$$\frac{1}{l_n}\frac{\partial}{\partial X}\left[\frac{-\sigma_{\text{eff,n}}}{l_n}\left(\frac{\partial\Phi'_{1,n}}{\partial X}\right)\right] - \frac{1}{l_n}\frac{\partial}{\partial X}\left[\frac{\kappa_{\text{eff,n}}}{l_n}\left(\frac{\partial\Phi'_{2,n}}{\partial X}\right)\right]$$
$$+\frac{1}{l_n}\frac{\partial}{\partial X}\left[\frac{2\kappa_{\text{eff,n}}RT}{Fc_0}\frac{(1-t_+)}{l_n}\left(\frac{\partial c'_n}{\partial X}\right)\right] = 0$$
$$\frac{1}{l_n}\frac{\partial}{\partial X}\left[\frac{-\sigma_{\text{eff,n}}}{l_n}\left(\frac{\partial\Phi''_{1,n}}{\partial X}\right)\right] - \frac{1}{l_n}\frac{\partial}{\partial X}\left[\frac{\kappa_{\text{eff,n}}}{l_n}\left(\frac{\partial\Phi''_{2,n}}{\partial X}\right)\right]$$
$$+\frac{1}{l_n}\frac{\partial}{\partial X}\left[\frac{2\kappa_{\text{eff,n}}RT}{Fc_0}\frac{(1-t_+)}{l_n}\left(\frac{\partial c''_n}{\partial X}\right)\right] = 0 \quad [A2]$$

$$\frac{1}{l_n}\frac{\partial}{\partial X}\left[\frac{\sigma_{\text{eff,n}}}{l_n}\frac{\partial}{\partial X}\Phi'_{1,n}\right] = a_n F\left(\frac{i0_n(\alpha_A+\alpha_C)}{RT}\left(\Phi'_{1,n}-\Phi'_{2,n}-dUdC_n * cns'\right)\right.$$
$$\left.-\frac{\omega Cdl_n}{F}\left(\Phi''_{1,n}-\Phi''_{2,n}\right)\right) \quad [A3]$$

$$\frac{1}{l_n}\frac{\partial}{\partial X}\left[\frac{\sigma_{\text{eff,n}}}{l_n}\frac{\partial}{\partial X}\Phi''_{1,n}\right] = a_n F\left(\frac{i0_n(\alpha_A+\alpha_C)}{RT}\left(\Phi''_{1,n}-\Phi''_{2,n}-dUdC_n * cns''\right)\right.$$
$$\left.+\frac{\omega Cdl_n}{F}\left(\Phi'_{1,n}-\Phi'_{2,n}\right)\right)$$

Boundary conditions at the anode current collector ($X = 0$) are given by:

$$\begin{aligned}
&\tfrac{\partial c'_n}{\partial X}|_{X=0} = 0\\
&\tfrac{\partial c''_n}{\partial X}|_{X=0} = 0\\
&\Phi'_{2,n}|_{X=0} = 0\\
&\Phi''_{2,n}|_{X=0} = 0\\
&\left(\tfrac{1}{l_n}\tfrac{\partial\Phi'_{1,n}}{\partial X}\right)\Big|_{X=0} = -\tfrac{I}{\sigma_{eff,n}}\\
&\left(\tfrac{1}{l_n}\tfrac{\partial\Phi''_{1,n}}{\partial X}\right)\Big|_{X=0} = 0
\end{aligned} \quad [A4]$$

Boundary Conditions at the anode-separator interface ($X = 1$) are:

$$\begin{aligned}
&\tfrac{-D_{\text{eff,n}}}{l_n}\tfrac{\partial c'_n}{\partial X}|_{X=1} = \tfrac{-D_{\text{eff,s}}}{l_s}\tfrac{\partial c'_s}{\partial X}|_{X=0}\\
&\tfrac{-D_{\text{eff,n}}}{l_n}\tfrac{\partial c''_n}{\partial X}|_{X=1} = \tfrac{-D_{\text{eff,s}}}{l_s}\tfrac{\partial c''_s}{\partial X}|_{X=0}\\
&\tfrac{-\kappa_{\text{eff,n}}}{l_n}\tfrac{\partial\Phi'_{2,n}}{\partial X}|_{X=1} = \tfrac{-\kappa_{\text{eff,s}}}{l_s}\tfrac{\partial\Phi'_{2,s}}{\partial X}|_{X=0}\\
&\tfrac{-\kappa_{\text{eff,n}}}{l_n}\tfrac{\partial\Phi''_{2,n}}{\partial X}|_{X=1} = \tfrac{-\kappa_{\text{eff,s}}}{l_s}\tfrac{\partial\Phi''_{2,s}}{\partial X}|_{X=0}\\
&\tfrac{\partial\Phi'_{1,n}}{\partial X}|_{X=1} = 0\\
&\tfrac{\partial\Phi''_{1,n}}{\partial X}|_{X=1} = 0
\end{aligned} \quad [A5]$$

The internal collocation point inside the negative electrode is chosen as the root of the first-order Jacobi polynomial in the scaled region $X \in [0, 1]$. The root lies at $X = \frac{1}{2}$.

Including the boundary points, the three points are now given as $X = \{0, \frac{1}{2}, 1\}$.

As mentioned previously, the variables are assumed to follow a polynomial profile. For example, the concentrations are given by:

$$\begin{aligned}
c'_n(X) &= A_0^n + A_1^n X + A_2^n X^2 = \sum_{i=0}^{2} A_i^n X^i\\
c''_n(X) &= B_0^n + B_1^n X + B_2^n X^2 = \sum_{i=0}^{2} B_i^n X^i
\end{aligned} \quad [A6]$$

Similarly, the potentials in each phase are represented by:

$$\Phi'_{1,n}(X) = C_0^n + C_1^n X + C_2^n X^2 = \sum_{i=0}^{2} C_i^n X^i \quad [A7]$$

$$\begin{aligned}
\Phi''_{1,n}(X) &= E_0^n + E_1^n X + E_2^n X^2 = \sum_{i=0}^{2} E_i^n X^i\\
\Phi'_{2,n}(X) &= Q_0^n + Q_1^n X + Q_2^n X^2 = \sum_{i=0}^{2} Q_i^n X^i\\
\Phi''_{2,n}(X) &= R_0^n + R_1^n X + R_2^n X^2 = \sum_{i=0}^{2} R_i^n X^i
\end{aligned} \quad [A8]$$

where A_i^n,B_i^n,C_i^n, E_i^n, Q_i^n and R_i^n are the coefficients of X^i, and the superscript 'n' denotes the values in the negative electrode region.

Table AI. Equations for the P2D impedance model for the full cell (*u'* represents the real-part of the variable *u*, and *u"* represents the imaginary part of the variable *u*).

Governing Equation	Boundary Conditions
Negative Electrode	
$-\varepsilon_n c''_n\omega = \frac{1}{l_n}\frac{\partial}{\partial X}\left[\frac{D_{\text{eff,n}}}{l_n}\frac{\partial c'_n}{\partial X}\right] + a_n(1-t_+)(j'_n + j'_{\text{dl,n}})$	$\frac{\partial c'_n}{\partial X}\vert_{X=0} = 0$
$\varepsilon_n c'_n\omega = \frac{1}{l_n}\frac{\partial}{\partial X}\left[\frac{D_{\text{eff,n}}}{l_n}\frac{\partial c''_n}{\partial X}\right] + a_n(1-t_+)(j''_n + j''_{\text{dl,n}})$	$\frac{\partial c''_n}{\partial X}\vert_{X=0} = 0$
	$\frac{-D_{\text{eff,n}}}{l_n}\frac{\partial c'_n}{\partial X}\vert_{X=1} = \frac{-D_{\text{eff,s}}}{l_s}\frac{\partial c'_s}{\partial X}\vert_{X=0}$
	$\frac{-D_{\text{eff,n}}}{l_n}\frac{\partial c''_n}{\partial X}\vert_{X=1} = \frac{-D_{\text{eff,s}}}{l_s}\frac{\partial c''_s}{\partial X}\vert_{X=0}$
$\frac{1}{l_n}\frac{\partial}{\partial X}\left[\frac{-\sigma_{\text{eff,n}}}{l_n}\left(\frac{\partial \Phi'_{1,n}}{\partial X}\right)\right] - \frac{1}{l_n}\frac{\partial}{\partial X}\left[\frac{\kappa_{\text{eff,n}}}{l_n}\left(\frac{\partial \Phi'_{2,n}}{\partial X}\right)\right]$	$\Phi'_{2,n}\vert_{X=0} = 0$
$+\frac{1}{l_n}\frac{\partial}{\partial X}\left[\frac{2\kappa_{\text{eff,n}}RT}{Fc_0}\frac{(1-t_+)}{l_n}\left(\frac{\partial c'_n}{\partial X}\right)\right] = 0$	
$\frac{1}{l_n}\frac{\partial}{\partial X}\left[\frac{-\sigma_{\text{eff,n}}}{l_n}\left(\frac{\partial \Phi''_{1,n}}{\partial X}\right)\right] - \frac{1}{l_n}\frac{\partial}{\partial X}\left[\frac{\kappa_{\text{eff,n}}}{l_n}\left(\frac{\partial \Phi''_{2,n}}{\partial X}\right)\right]$	$\Phi''_{2,n}\vert_{X=0} = 0$
$+\frac{1}{l_n}\frac{\partial}{\partial X}\left[\frac{2\kappa_{\text{eff,n}}RT}{Fc_0}\frac{(1-t_+)}{l_n}\left(\frac{\partial c''_n}{\partial X}\right)\right] = 0$	
	$\frac{-\kappa_{\text{eff,n}}}{l_n}\frac{\partial \Phi'_{2,n}}{\partial X}\vert_{X=1} = \frac{-\kappa_{\text{eff,s}}}{l_s}\frac{\partial \Phi'_{2,s}}{\partial X}\vert_{X=0}$
	$\frac{-\kappa_{\text{eff,n}}}{l_n}\frac{\partial \Phi''_{2,n}}{\partial X}\vert_{X=1} = \frac{-\kappa_{\text{eff,s}}}{l_s}\frac{\partial \Phi''_{2,s}}{\partial X}\vert_{X=0}$
$\frac{1}{l_n}\frac{\partial}{\partial X}\left[\frac{\sigma_{\text{eff,n}}}{l_n}\frac{\partial}{\partial X}\Phi'_{1,n}\right] = a_n F(j'_n + j'_{dl,n})$	$(\frac{1}{l_n}\frac{\partial \Phi'_{1,n}}{\partial X})\vert_{X=0} = -\frac{I}{\sigma_{eff,n}}$
$\frac{1}{l_n}\frac{\partial}{\partial X}\left[\frac{\sigma_{\text{eff,n}}}{l_n}\frac{\partial}{\partial X}\Phi''_{1,n}\right] = a_n F(j''_n + j''_{dl,n})$	$(\frac{1}{l_n}\frac{\partial \Phi''_{1,n}}{\partial X})\vert_{X=0} = 0$
	$\frac{\partial \Phi'_{1,n}}{\partial X}\vert_{X=1} = 0$
	$\frac{\partial \Phi''_{1,n}}{\partial X}\vert_{X=1} = 0$
$-\omega c^{s''}_n = \frac{1}{r^2}\frac{\partial}{\partial r}\left[r^2 D^s_n \frac{\partial c^{s'}_n}{\partial r}\right]$	$\frac{\partial c^{s'}_n}{\partial r}\vert_{r=0} = 0$
$\omega c^{s'}_n = \frac{1}{r^2}\frac{\partial}{\partial r}\left[r^2 D^s_n \frac{\partial c^{s''}_n}{\partial r}\right]$	$\frac{\partial c^{s''}_n}{\partial r}\vert_{r=0} = 0$
	$-D^s_n \frac{\partial c^{s'}_n}{\partial r}\vert_{r=R_n} = j'_n$
	$-D^s_n \frac{\partial c^{s''}_n}{\partial r}\vert_{r=R_n} = j''_n$
Separator	
$-\varepsilon_s c''_s\omega = \frac{1}{l_s}\frac{\partial}{\partial X}\left[\frac{D_{\text{eff,s}}}{l_s}\frac{\partial c'_s}{\partial X}\right]$	$c'_n\vert_{X=1} = c'_s\vert_{X=0}$
$\varepsilon_s c'_s\omega = \frac{1}{l_s}\frac{\partial}{\partial X}\left[\frac{D_{\text{eff,s}}}{l_s}\frac{\partial c''_s}{\partial X}\right]$	$c''_n\vert_{X=1} = c''_s\vert_{X=0}$
	$c'_s\vert_{X=1} = c'_p\vert_{X=0}$
	$c''_s\vert_{X=1} = c''_p\vert_{X=0}$
$-\frac{1}{l_s}\frac{\partial}{\partial X}\left[\frac{\kappa_{\text{eff,s}}}{l_s}\left(\frac{\partial \Phi'_{2,s}}{\partial X}\right)\right] + \frac{1}{l_s}\frac{\partial}{\partial X}\left[\frac{2\kappa_{\text{eff,s}}RT}{Fc_0}\frac{(1-t_+)}{l_s}\left(\frac{\partial c'_s}{\partial X}\right)\right] = 0$	$\Phi'_{2,n}\vert_{X=1} = \Phi'_{2,s}\vert_{X=0}$
$-\frac{1}{l_s}\frac{\partial}{\partial X}\left[\frac{\kappa_{\text{eff,s}}}{l_s}\left(\frac{\partial \Phi''_{2,s}}{\partial X}\right)\right] + \frac{1}{l_s}\frac{\partial}{\partial X}\left[\frac{2\kappa_{\text{eff,s}}RT}{Fc_0}\frac{(1-t_+)}{l_s}\left(\frac{\partial c''_s}{\partial X}\right)\right] = 0$	$\Phi''_{2,n}\vert_{X=1} = \Phi''_{2,s}\vert_{X=0}$
	$\Phi'_{2,s}\vert_{X=1} = \Phi'_{2,p}\vert_{X=0}$
	$\Phi''_{2,s}\vert_{X=1} = \Phi''_{2,p}\vert_{X=0}$
	$\frac{-D_{\text{eff,s}}}{l_s}\frac{\partial c'_s}{\partial X}\vert_{X=1} = \frac{-D_{\text{eff,p}}}{l_p}\frac{\partial c'_p}{\partial X}\vert_{X=0}$
	$\frac{-D_{\text{eff,s}}}{l_s}\frac{\partial c''_s}{\partial X}\vert_{X=1} = \frac{-D_{\text{eff,p}}}{l_p}\frac{\partial c''_p}{\partial X}\vert_{X=0}$
Positive Electrode	$\frac{\partial c'_p}{\partial X}\vert_{X=1} = 0$
$-\varepsilon_p c''_p\omega = \frac{1}{l_p}\frac{\partial}{\partial X}\left[\frac{D_{\text{eff,p}}}{l_p}\frac{\partial c'_p}{\partial X}\right] + a_p(1-t_+)(j'_p + j'_{\text{dl,p}})$	$\frac{\partial c''_p}{\partial X}\vert_{X=1} = 0$
$\varepsilon_p c'_p\omega = \frac{1}{l_p}\frac{\partial}{\partial X}\left[\frac{D_{\text{eff,p}}}{l_p}\frac{\partial c''_p}{\partial X}\right] + a_p(1-t_+)(j''_p + j''_{\text{dl,p}})$	
	$\frac{-\kappa_{\text{eff,s}}}{l_s}\frac{\partial \Phi'_{2,s}}{\partial X}\vert_{X=1} = \frac{-\kappa_{\text{eff,p}}}{l_p}\frac{\partial \Phi'_{2,p}}{\partial X}\vert_{X=0}$
	$\frac{-\kappa_{\text{eff,s}}}{l_s}\frac{\partial \Phi''_{2,s}}{\partial X}\vert_{X=1} = \frac{-\kappa_{\text{eff,p}}}{l_p}\frac{\partial \Phi''_{2,p}}{\partial X}\vert_{X=0}$
	$\frac{\partial \Phi'_{2,p}}{\partial X}\vert_{X=1} = 0$
	$\frac{\partial \Phi''_{2,p}}{\partial X}\vert_{X=1} = 0$
$\frac{1}{l_p}\frac{\partial}{\partial X}\left[\frac{-\sigma_{\text{eff,p}}}{l_p}\left(\frac{\partial \Phi'_{1,p}}{\partial X}\right)\right] - \frac{1}{l_p}\frac{\partial}{\partial X}\left[\frac{\kappa_{\text{eff,p}}}{l_p}\left(\frac{\partial \Phi'_{2,p}}{\partial X}\right)\right]$	$\frac{\partial \Phi'_{1,p}}{\partial X}\vert_{X=0} = 0$
$+\frac{1}{l_p}\frac{\partial}{\partial X}\left[\frac{2\kappa_{\text{eff,p}}RT}{Fc_0}\frac{(1-t_+)}{l_p}\left(\frac{\partial c'_p}{\partial X}\right)\right] = 0$	
$\frac{1}{l_p}\frac{\partial}{\partial X}\left[\frac{-\sigma_{\text{eff,p}}}{l_p}\left(\frac{\partial \Phi''_{1,p}}{\partial X}\right)\right] - \frac{1}{l_p}\frac{\partial}{\partial X}\left[\frac{\kappa_{\text{eff,p}}}{l_p}\left(\frac{\partial \Phi''_{2,p}}{\partial X}\right)\right]$	$\frac{\partial \Phi''_{1,p}}{\partial X}\vert_{X=0} = 0$
$+\frac{1}{l_p}\frac{\partial}{\partial X}\left[\frac{2\kappa_{\text{eff,p}}RT}{Fc_0}\frac{(1-t_+)}{l_p}\left(\frac{\partial c''_p}{\partial X}\right)\right] = 0$	
	$(\frac{1}{l_p}\frac{\partial \Phi'_{1,p}}{\partial X})\vert_{X=1} = -\frac{I}{\sigma_{eff,p}}$
	$(\frac{1}{l_p}\frac{\partial \Phi''_{1,p}}{\partial X})\vert_{X=1} = 0$
$\frac{1}{l_p}\frac{\partial}{\partial X}\left[\frac{\sigma_{\text{eff,p}}}{l_p}\frac{\partial}{\partial X}\Phi'_{1,p}\right] = a_p F(j'_p + j'_{\text{dl,p}})$	
$\frac{1}{l_p}\frac{\partial}{\partial X}\left[\frac{\sigma_{\text{eff,p}}}{l_p}\frac{\partial}{\partial X}\Phi''_{1,p}\right] = a_p F(j''_p + j''_{\text{dl,p}})$	
$-\omega c^{s''}_p = \frac{1}{r^2}\frac{\partial}{\partial r}\left[r^2 D^s_p \frac{\partial c^{s'}_p}{\partial r}\right]$	$\frac{\partial c^{s'}_p}{\partial r}\vert_{r=0} = 0$
$\omega c^{s'}_p = \frac{1}{r^2}\frac{\partial}{\partial r}\left[r^2 D^s_p \frac{\partial c^{s''}_p}{\partial r}\right]$	$\frac{\partial c^{s''}_p}{\partial r}\vert_{r=0} = 0$
	$-D^s_p \frac{\partial c^{s'}_p}{\partial r}\vert_{r=R_p} = j'_p$
	$-D^s_p \frac{\partial c^{s''}_p}{\partial r}\vert_{r=R_p} = j''_p$

Table AII. Additional Equations.

$$\eta'_p = \Phi'_{1,p} - \Phi'_{2,p} - dUdC_p * cps'$$
$$\eta''_p = \Phi''_{1,p} - \Phi''_{2,p} - dUdC_p * cps''$$
$$cps' = c_p^{s\,\prime}|_{r=R_p}$$
$$cps'' = c_p^{s\,\prime\prime}|_{r=R_p}$$
$$j'_p = \frac{i0_p(\alpha_A+\alpha_C)}{RT}\eta'_p$$
$$j''_p = \frac{i0_p(\alpha_A+\alpha_C)}{RT}\eta''_p$$
$$j'_{dl,p} = -\frac{\omega Cdl_p}{F}(\Phi''_{1,p} - \Phi''_{2,p})$$
$$j''_{dl,p} = \frac{\omega Cdl_p}{F}(\Phi'_{1,p} - \Phi'_{2,p})$$
$$\eta'_n = \Phi'_{1,n} - \Phi'_{2,n} - dUdC_n * cns'$$
$$\eta''_n = \Phi''_{1,n} - \Phi''_{2,n} - dUdC_n * cns''$$
$$cns' = c_n^{s\,\prime}|_{r=R_n}$$
$$cns'' = c_n^{s\,\prime\prime}|_{r=R_n}$$
$$j'_n = \frac{i0_n(\alpha_A+\alpha_C)}{RT}\eta'_n$$
$$j''_n = \frac{i0_n(\alpha_A+\alpha_C)}{RT}\eta''_n$$
$$j'_{dl,n} = -\frac{\omega Cdl_n}{F}(\Phi''_{1,n} - \Phi''_{2,n})$$
$$j''_{dl,n} = \frac{\omega Cdl_n}{F}(\Phi'_{1,n} - \Phi'_{2,n})$$
$$D_{eff,p} = D\varepsilon_p^{Brugg}$$
$$D_{eff,s} = D\varepsilon_s^{Brugg}$$
$$D_{eff,n} = D\varepsilon_n^{Brugg}$$
$$\kappa_{eff,p} = \kappa\varepsilon_p^{Brugg}$$
$$\kappa_{eff,s} = \kappa\varepsilon_s^{Brugg}$$
$$\kappa_{eff,n} = \kappa\varepsilon_n^{Brugg}$$
$$\sigma_{eff,p} = \sigma_p(1-\varepsilon_p-\varepsilon_{f,p})^{Brugg}$$
$$\sigma_{eff,n} = \sigma_n(1-\varepsilon_n-\varepsilon_{f,n})^{Brugg}$$

Values of the real and imaginary parts of each of the variables are assumed at these three node points as:

$$\begin{aligned}
c'_n(X) &= \{c'_{n,1}, c'_{n,2}, c'_{n,3}\}\\
c''_n(X) &= \{c''_{n,1}, c''_{n,2}, c''_{n,3}\}\\
\Phi'_{1,n}(X) &= \{\varphi'_{n,1}, \varphi'_{n,2}, \varphi'_{n,3}\}\\
\Phi''_{1,n}(X) &= \{\varphi''_{n,1}, \varphi''_{n,2}, \varphi''_{n,3}\}\\
\Phi'_{2,n}(X) &= \{\psi'_{n,1}, \psi'_{n,2}, \psi'_{n,3}\}\\
\Phi''_{2,n}(X) &= \{\psi''_{n,1}, \psi''_{n,2}, \psi''_{n,3}\}
\end{aligned} \quad [A9]$$

Substituting the values of X in Equation A6, the following relations can be easily derived.

$$\begin{aligned}
c'_{n,1} &= A_0^n + A_1^n(0) + A_2^n(0)^2 = A_0^n\\
c'_{n,2} &= A_0^n + A_1^n*\left(\tfrac{1}{2}\right) + A_2^n*\left(\tfrac{1}{2}\right)^2\\
c'_{n,3} &= A_0^n + A_1^n*(1) + A_2^n*(1)^2
\end{aligned} \quad [A10]$$

The coefficients A_0^n, A_1^n, A_2^n can easily be solved in terms of $c'_{n,1}, c'_{n,2}, c'_{n,3}$. Similar equations are obtained for other variables.

$$\begin{aligned}
c''_{n,1} &= B_0^n + B_1^n(0) + B_2^n(0)^2 = B_0^n\\
c''_{n,2} &= B_0^n + B_1^n*\left(\tfrac{1}{2}\right) + B_2^n*\left(\tfrac{1}{2}\right)^2\\
c''_{n,3} &= B_0^n + B_1^n*(1) + B_2^n*(1)^2
\end{aligned} \quad [A11]$$

$$\begin{aligned}
\varphi'_{n,1} &= C_0^n\\
\varphi'_{n,2} &= C_0^n + C_1^n*\left(\tfrac{1}{2}\right) + C_2^n*\left(\tfrac{1}{2}\right)^2\\
\varphi'_{n,3} &= C_0^n + C_1^n*(1) + C_2^n*(1)^2
\end{aligned} \quad [A12]$$

$$\begin{aligned}
\varphi''_{n,1} &= E_0^n\\
\varphi''_{n,2} &= E_0^n + E_1^n*\left(\tfrac{1}{2}\right) + E_2^n*\left(\tfrac{1}{2}\right)^2\\
\varphi''_{n,3} &= E_0^n + E_1^n*(1) + E_2^n*(1)^2
\end{aligned} \quad [A13]$$

$$\begin{aligned}
\psi'_{n,1} &= Q_0^n\\
\psi'_{n,2} &= Q_0^n + Q_1^n*\left(\tfrac{1}{2}\right) + Q_2^n*\left(\tfrac{1}{2}\right)^2\\
\psi'_{n,3} &= Q_0^n + Q_1^n*(1) + Q_2^n*(1)^2
\end{aligned} \quad [A14]$$

$$\begin{aligned}
\psi''_{n,1} &= R_0^n\\
\psi''_{n,2} &= R_0^n + R_1^n*\left(\tfrac{1}{2}\right) + R_2^n*\left(\tfrac{1}{2}\right)^2\\
\psi''_{n,3} &= R_0^n + R_1^n*(1) + R_2^n*(1)^2
\end{aligned} \quad [A15]$$

Equations A11–A15 can be used to eliminate all the coefficients B_i^n, C_i^n, E_i^n, Q_i^n and R_i^n in terms of the variables at the specific node points, as shown in the right hand side of Equation A9.

Equations A6–A8 are substituted in the governing Equations A1–A3 to get:

$$-\varepsilon_n\left(\sum_{i=0}^{2} B_i^n X^i\right)\omega = \frac{1}{l_n}\left[\frac{D_{\text{eff,n}}}{l_n}\left(2A_2^n\right)\right] + a_n(1-t_+)\left(\frac{i0_n(\alpha_A+\alpha_C)}{RT}\left(\left(\sum_{i=0}^{2} C_i^n X^i\right) - \left(\sum_{i=0}^{2} Q_i^n X^i\right) - dUdC_n * cns'\right) - \frac{\omega Cdl_n}{F}\left(\left(\sum_{i=0}^{2} E_i^n X^i\right) - \left(\sum_{i=0}^{2} R_i^n X^i\right)\right)\right) \quad [A16]$$

$$\varepsilon_n\left(\sum_{i=0}^{2} A_i^n X^i\right)\omega = \frac{1}{l_n}\left[\frac{D_{\text{eff,n}}}{l_n}\left(2B_2^n\right)\right] + a_n(1-t_+)\left(\frac{i0_n(\alpha_A+\alpha_C)}{RT}\left(\left(\sum_{i=0}^{2} E_i^n X^i\right) - \left(\sum_{i=0}^{2} R_i^n X^i\right) - dUdC_n * cns''\right) + \frac{\omega Cdl_n}{F}\left(\left(\sum_{i=0}^{2} C_i^n X^i\right) - \left(\sum_{i=0}^{2} Q_i^n X^i\right)\right)\right)$$

Table AIII. List of parameters.

Symbol	Parameter	Positive Electrode	Separator	Negative Electrode	Units
σ_i	Solid phase conductivity	100	-	100	S/m
$\varepsilon_{f,i}$	Filler fraction	0.025	-	0.0326	
ε_i	Porosity	0.385	0.724	0.485	
Brugg	Bruggeman Coefficient	4	4	4	
D	Electrolyte diffusivity	7.5×10^{-10}	7.5×10^{-10}	7.5×10^{-10}	m^2/s
κ	Electrolyte conductivity	0.204737	0.204737	0.204737	S/m
D_i^s	Solid Phase Diffusivity	1.0×10^{-14}	-	3.9×10^{-14}	m^2/s
$i0_i$	Exchange current density of the reaction	3.67	-	3.30	A/m^2
c_0	Initial electrolyte concentration	1000	1000	1000	mol/m^3
$R_{p,i}$	Particle Radius	2.0×10^{-6}	-	2.0×10^{-6}	m
a_i	Particle Surface Area to Volume	885000	-	723600	m^2/m^3
l_i	Region thickness	80×10^{-6}	25×10^{-6}	88×10^{-6}	m
t_+	Transference number	0.364	0.364	0.364	
α_i	Charge transfer coefficient	0.5	-	0.5	
$dUdC_i$	First derivative of open-circuit potential	-11.6724×10^{-6}		-3.21038×10^{-6}	$V.m^3/mol$
Cdl_i	Double-layer capacitance	10		10	$\mu F/cm^2$
F	Faraday's Constant		96487		C/mol
T	Temperature	298	298	298	K
R	Gas Constant		8.314		J/mol/ K
I	Applied Current	1	1	1	A/m^2

Table AIV. Governing Equations and Boundary conditions for a cathode-lithium half cell.

Region	Governing Equations/Boundary Conditions
Lithium-Separator interface	$\frac{-D_{\text{eff,s}}}{l_s}\frac{\partial c'_s}{\partial X}\vert_{X=0} = \frac{-I(1-t_+)}{F}$
	$\frac{-D_{\text{eff,s}}}{l_s}\frac{\partial c''_s}{\partial X}\vert_{X=0} = 0$
	$\Phi'_{2,n}\vert_{X=0} = 0$
	$\Phi''_{2,n}\vert_{X=0} = 0$
Separator	$-\varepsilon_s c''_s\omega = \frac{1}{l_s}\frac{\partial}{\partial X}\left[\frac{D_{\text{eff,s}}}{l_s}\frac{\partial c'_s}{\partial X}\right]$
	$\varepsilon_s c'_s\omega = \frac{1}{l_s}\frac{\partial}{\partial X}\left[\frac{D_{\text{eff,s}}}{l_s}\frac{\partial c''_s}{\partial X}\right]$
	$-\frac{1}{l_s}\frac{\partial}{\partial X}\left[\frac{\kappa_{\text{eff,s}}}{l_s}\left(\frac{\partial \Phi'_{2,s}}{\partial X}\right)\right] + \frac{1}{l_s}\frac{\partial}{\partial X}\left[\frac{2\kappa_{\text{eff,s}}RT}{Fc_0}\frac{(1-t_+)}{l_s}\left(\frac{\partial c'_s}{\partial X}\right)\right] = 0$
	$-\frac{1}{l_s}\frac{\partial}{\partial X}\left[\frac{\kappa_{\text{eff,s}}}{l_s}\left(\frac{\partial \Phi''_{2,s}}{\partial X}\right)\right] + \frac{1}{l_s}\frac{\partial}{\partial X}\left[\frac{2\kappa_{\text{eff,s}}RT}{Fc_0}\frac{(1-t_+)}{l_s}\left(\frac{\partial c''_s}{\partial X}\right)\right] = 0$
Separator-Cathode interface	$\frac{-D_{\text{eff,s}}}{l_s}\frac{\partial c'_s}{\partial X}\vert_{X=1} = \frac{-D_{\text{eff,p}}}{l_p}\frac{\partial c'_p}{\partial X}\vert_{X=0}$
	$\frac{-D_{\text{eff,s}}}{l_s}\frac{\partial c''_s}{\partial X}\vert_{X=1} = \frac{-D_{\text{eff,p}}}{l_p}\frac{\partial c''_p}{\partial X}\vert_{X=0}$
	$\frac{-\kappa_{\text{eff,s}}}{l_s}\frac{\partial \Phi'_{2,s}}{\partial X}\vert_{X=1} = \frac{-\kappa_{\text{eff,p}}}{l_p}\frac{\partial \Phi'_{2,p}}{\partial X}\vert_{X=0}$
	$\frac{-\kappa_{\text{eff,s}}}{l_s}\frac{\partial \Phi''_{2,s}}{\partial X}\vert_{X=1} = \frac{-\kappa_{\text{eff,p}}}{l_p}\frac{\partial \Phi''_{2,p}}{\partial X}\vert_{X=0}$
	$\frac{\partial \Phi'_{1,p}}{\partial X}\vert_{X=0} = 0$
	$\frac{\partial \Phi''_{1,p}}{\partial X}\vert_{X=0} = 0$
	$c'_s\vert_{X=1} = c'_p\vert_{X=0}$
	$c''_s\vert_{X=1} = c''_p\vert_{X=0}$
	$\Phi'_{2,s}\vert_{X=1} = \Phi'_{2,p}\vert_{X=0}$
	$\Phi''_{2,s}\vert_{X=1} = \Phi''_{2,p}\vert_{X=0}$
Cathode	$-\varepsilon_p c''_p\omega = \frac{1}{l_p}\frac{\partial}{\partial X}\left[\frac{D_{\text{eff,p}}}{l_p}\frac{\partial c'_p}{\partial X}\right] + a_p(1-t_+)(j'_p + j'_{\text{dl,p}})$
	$\varepsilon_p c'_p\omega = \frac{1}{l_p}\frac{\partial}{\partial X}\left[\frac{D_{\text{eff,p}}}{l_p}\frac{\partial c''_p}{\partial X}\right] + a_p(1-t_+)(j''_p + j''_{\text{dl,p}})$
	$\frac{1}{l_p}\frac{\partial}{\partial X}\left[\frac{-\sigma_{\text{eff,p}}}{l_p}\left(\frac{\partial \Phi'_{1,p}}{\partial X}\right)\right] - \frac{1}{l_p}\frac{\partial}{\partial X}\left[\frac{\kappa_{\text{eff,p}}}{l_p}\left(\frac{\partial \Phi'_{2,p}}{\partial X}\right)\right]$ $+\frac{1}{l_p}\frac{\partial}{\partial X}\left[\frac{2\kappa_{\text{eff,p}}RT}{Fc_0}\frac{(1-t_+)}{l_p}\left(\frac{\partial c'_p}{\partial X}\right)\right] = 0$
	$\frac{1}{l_p}\frac{\partial}{\partial X}\left[\frac{-\sigma_{\text{eff,p}}}{l_p}\left(\frac{\partial \Phi''_{1,p}}{\partial X}\right)\right] - \frac{1}{l_p}\frac{\partial}{\partial X}\left[\frac{\kappa_{\text{eff,p}}}{l_p}\left(\frac{\partial \Phi''_{2,p}}{\partial X}\right)\right]$ $+\frac{1}{l_p}\frac{\partial}{\partial X}\left[\frac{2\kappa_{\text{eff,p}}RT}{Fc_0}\frac{(1-t_+)}{l_p}\left(\frac{\partial c''_p}{\partial X}\right)\right] = 0$
	$\frac{1}{l_p}\frac{\partial}{\partial X}\left[\frac{\sigma_{\text{eff,p}}}{l_p}\frac{\partial}{\partial X}\Phi'_{1,p}\right] = a_p F(j'_p + j'_{\text{dl,p}})$
	$\frac{1}{l_p}\frac{\partial}{\partial X}\left[\frac{\sigma_{\text{eff,p}}}{l_p}\frac{\partial}{\partial X}\Phi''_{1,p}\right] = a_p F(j''_p + j''_{\text{dl,p}})$
	$-\omega c_p^{s''} = \frac{1}{r^2}\frac{\partial}{\partial r}\left[r^2 D_p^s\frac{\partial c_p^{s'}}{\partial r}\right]$
	$\omega c_p^{s'} = \frac{1}{r^2}\frac{\partial}{\partial r}\left[r^2 D_p^s\frac{\partial c_p^{s''}}{\partial r}\right]$
Cathode-current collector interface	$\frac{\partial c'_p}{\partial X}\vert_{X=1} = 0$
	$\frac{\partial c''_p}{\partial X}\vert_{X=1} = 0$
	$\frac{\partial \Phi'_{2,p}}{\partial X}\vert_{X=1} = 0$
	$\frac{\partial \Phi''_{2,p}}{\partial X}\vert_{X=1} = 0$
	$(\frac{1}{l_p}\frac{\partial \Phi'_{1,p}}{\partial X})\vert_{X=1} = -\frac{I}{\sigma_{eff,p}}$
	$(\frac{1}{l_p}\frac{\partial \Phi''_{1,p}}{\partial X})\vert_{X=1} = 0$

Table AV. List of parameters for a different chemistry with different cell design.

Symbol	Parameter	Positive Electrode	Separator	Units
σ_i	Solid phase conductivity	3.8	-	S/m
$\varepsilon_{f,i}$	Filler fraction	0.214	-	
ε_i	Porosity	0.416	0.593	
Brugg	Bruggeman Coefficient	5.2	2.4	
D	Electrolyte diffusivity	3.35×10^{-10}	3.35×10^{-10}	m^2/s
κ	Electrolyte conductivity	0.98	0.98	S/m
D_i^s	Solid Phase Diffusivity	1.0×10^{-13}	-	m^2/s
$i0_i$	Exchange current density of the reaction	4.16	-	A/m^2
c_0	Initial electrolyte concentration	1000	1000	mol/m^3
$R_{p,i}$	Particle Radius	8.5×10^{-6}	-	m
a_i	Particle Surface Area to Volume	130588	-	m^2/m^3
l_i	Region thickness	144.4×10^{-6}	76×10^{-6}	m
t_+	Transference number	0.363	0.363	

$$\begin{aligned}&\tfrac{1}{l_n}\left[\tfrac{-\sigma_{\text{eff,n}}}{l_n}\left(2C_2^n\right)\right]-\tfrac{1}{l_n}\left[\tfrac{\kappa_{\text{eff,n}}}{l_n}\left(2Q_2^n\right)\right]+\tfrac{1}{l_n}\left[\tfrac{2\kappa_{\text{eff,n}}RT}{Fc_0}\tfrac{(1-t_+)}{l_n}\left(2A_2^n\right)\right]=0\\&\tfrac{1}{l_n}\left[\tfrac{-\sigma_{\text{eff,n}}}{l_n}\left(2E_2^n\right)\right]-\tfrac{1}{l_n}\left[\tfrac{\kappa_{\text{eff,n}}}{l_n}\left(2R_2^n\right)\right]+\tfrac{1}{l_n}\left[\tfrac{2\kappa_{\text{eff,n}}RT}{Fc_0}\tfrac{(1-t_+)}{l_n}\left(2B_2^n\right)\right]=0\end{aligned} \quad [A17]$$

$$\begin{aligned}\frac{1}{l_n}\left[\frac{\sigma_{\text{eff,n}}}{l_n}\left(2C_2^n\right)\right]&=a_nF\left(\frac{i0_n\left(\alpha_A+\alpha_C\right)}{RT}\left(\left(\sum_{i=0}^{2}C_i^nX^i\right)-\left(\sum_{i=0}^{2}Q_i^nX^i\right)\right.\right.\\&\left.\left.-dUdC_n*cns'\right)-\frac{\omega Cdl_n}{F}\left(\left(\sum_{i=0}^{2}E_i^nX^i\right)-\left(\sum_{i=0}^{2}R_i^nX^i\right)\right)\right)\end{aligned} \quad [A18]$$

$$\begin{aligned}\frac{1}{l_n}\left[\frac{\sigma_{\text{eff,n}}}{l_n}\left(2E_2^n\right)\right]&=a_nF\left(\frac{i0_n\left(\alpha_A+\alpha_C\right)}{RT}\left(\left(\sum_{i=0}^{2}E_i^nX^i\right)-\left(\sum_{i=0}^{2}R_i^nX^i\right)\right.\right.\\&\left.\left.-dUdC_n*cns''\right)+\frac{\omega Cdl_n}{F}\left(\left(\sum_{i=0}^{2}C_i^nX^i\right)-\left(\sum_{i=0}^{2}Q_i^nX^i\right)\right)\right)\end{aligned}$$

Where cns' and cns'' are the real and imaginary parts of the surface concentrations of the particle in the solid-phase respectively, and are given by the analytical solution of the coupled solid-phase equations, in the radial direction.

Equations A16–A18 are valid at the internal collocation points, and hence the values of X ($X = \frac{1}{2}$) is substituted in A16–A18. Further, Equations A10–A15 can be used to get:

$$\begin{aligned}-\varepsilon_{\text{n}}\left(c''_{n,2}\right)\omega&=\frac{1}{l_n}\left[\frac{D_{\text{eff,n}}}{l_n}\left(2A_2^n\right)\right]+a_{\text{n}}\left(1-t_+\right)\left(\frac{i0_n\left(\alpha_A+\alpha_C\right)}{RT}\left(\left(\varphi'_{n,2}\right)-\left(\psi'_{n,2}\right)\right.\right.\\&\left.\left.-dUdC_n*cns'\right)-\frac{\omega Cdl_n}{F}\left(\left(\varphi''_{n,2}\right)-\left(\psi''_{n,2}\right)\right)\right)\end{aligned} \quad [A19]$$

$$\begin{aligned}\varepsilon_{\text{n}}\left(c'_{n,2}\right)\omega&=\frac{1}{l_n}\left[\frac{D_{\text{eff,n}}}{l_n}\left(2B_2^n\right)\right]+a_{\text{n}}\left(1-t_+\right)\left(\frac{i0_n\left(\alpha_A+\alpha_C\right)}{RT}\left(\left(\varphi''_{n,2}\right)-\left(\psi''_{n,2}\right)\right.\right.\\&\left.\left.-dUdC_n*cns''\right)+\frac{\omega Cdl_n}{F}\left(\left(\varphi'_{n,2}\right)-\left(\psi'_{n,2}\right)\right)\right)\end{aligned}$$

$$\begin{aligned}&\tfrac{1}{l_n}\left[\tfrac{-\sigma_{\text{eff,n}}}{l_n}\left(2C_2^n\right)\right]-\tfrac{1}{l_n}\left[\tfrac{\kappa_{\text{eff,n}}}{l_n}\left(2Q_2^n\right)\right]+\tfrac{1}{l_n}\left[\tfrac{2\kappa_{\text{eff,n}}RT}{Fc_0}\tfrac{(1-t_+)}{l_n}\left(2A_2^n\right)\right]=0\\&\tfrac{1}{l_n}\left[\tfrac{-\sigma_{\text{eff,n}}}{l_n}\left(2E_2^n\right)\right]-\tfrac{1}{l_n}\left[\tfrac{\kappa_{\text{eff,n}}}{l_n}\left(2R_2^n\right)\right]+\tfrac{1}{l_n}\left[\tfrac{2\kappa_{\text{eff,n}}RT}{Fc_0}\tfrac{(1-t_+)}{l_n}\left(2B_2^n\right)\right]=0\end{aligned} \quad [A20]$$

$$\begin{aligned}\frac{1}{l_n}\left[\frac{\sigma_{\text{eff,n}}}{l_n}\left(2C_2^n\right)\right]&=a_{\text{n}}F\left(\frac{i0_n\left(\alpha_A+\alpha_C\right)}{RT}\left(\left(\varphi'_{n,2}\right)-\left(\psi'_{n,2}\right)-dUdC_n*cns'\right)\right.\\&\left.-\frac{\omega Cdl_n}{F}\left(\left(\varphi''_{n,2}\right)-\left(\psi''_{n,2}\right)\right)\right)\end{aligned} \quad [A21]$$

$$\begin{aligned}\frac{1}{l_n}\left[\frac{\sigma_{\text{eff,n}}}{l_n}\left(2E_2^n\right)\right]&=a_{\text{n}}F\left(\frac{i0_n\left(\alpha_A+\alpha_C\right)}{RT}\left(\left(\varphi''_{n,2}\right)-\left(\psi''_{n,2}\right)-dUdC_n*cns''\right)\right.\\&\left.+\frac{\omega Cdl_n}{F}\left(\left(\varphi'_{n,2}\right)-\left(\psi'_{n,2}\right)\right)\right)\end{aligned}$$

It should be noted that Equation A20 remains the same as Equation A17 in this case, as there is no X term in Equation A17. However, when collocation for higher internal node points is considered, Equation A20 will have more terms owing to more number of roots of the resulting higher order polynomial.

At the boundary points ($X = 0$ *and* $X = 1$), the boundary conditions A4–A5 give additional sets of equations for each variable. Equations A6–A8 can be used in the boundary conditions to get:

$$\begin{aligned}&A_1^n=0\\&B_1^n=0\\&Q_1^n=0\\&R_1^n=0\\&\tfrac{1}{l_n}C_1^n=-\tfrac{I}{\sigma_{eff,n}}\\&E_1^n=0\end{aligned} \quad [A22]$$

$$\begin{aligned}&\tfrac{-D_{\text{eff,n}}}{l_n}\left(A_1^n+2A_2^n(1)\right)=\tfrac{-D_{\text{eff,s}}}{l_s}\left(A_1^s\right)\\&\tfrac{-D_{\text{eff,n}}}{l_n}\left(B_1^n+2B_2^n(1)\right)=\tfrac{-D_{\text{eff,s}}}{l_s}\left(B_1^s\right)\\&\tfrac{-\kappa_{\text{eff,n}}}{l_n}\left(Q_1^n+2Q_2^n(1)\right)=\tfrac{-\kappa_{\text{eff,s}}}{l_s}\left(Q_1^s\right)\\&\tfrac{-\kappa_{\text{eff,n}}}{l_n}\left(R_1^n+2R_2^n(1)\right)=\tfrac{-\kappa_{\text{eff,s}}}{l_s}\left(R_1^s\right)\\&C_1^n+2C_2^n(1)=0\\&E_1^n+2E_2^n(1)=0\end{aligned} \quad [A23]$$

Equations in the separator.—A similar treatment as done in the negative electrode can be done to obtain the resulting equations in the separator region. For the sake of brevity, below we only show the resulting equations in the separator region.

$$\begin{aligned}&c'_{s,1}=A_0^s\\&c'_{s,2}=A_0^s+A_1^s*\left(\tfrac{1}{2}\right)+A_2^s*\left(\tfrac{1}{2}\right)^2\\&c'_{s,3}=A_0^s+A_1^s*(1)+A_2^s*(1)^2\end{aligned} \quad [A24]$$

$$\begin{aligned}&c''_{s,1}=B_0^s\\&c''_{s,2}=B_0^s+B_1^s*\left(\tfrac{1}{2}\right)+B_2^s*\left(\tfrac{1}{2}\right)^2\\&c''_{s,3}=B_0^s+B_1^s*(1)+B_2^s*(1)^2\end{aligned} \quad [A25]$$

$$\begin{aligned}&\varphi'_{s,1}=C_0^s\\&\varphi'_{s,2}=C_0^s+C_1^s*\left(\tfrac{1}{2}\right)+C_2^s*\left(\tfrac{1}{2}\right)^2\\&\varphi'_{s,3}=C_0^s+C_1^s*(1)+C_2^s*(1)^2\end{aligned} \quad [A26]$$

$$\begin{aligned}&\varphi''_{s,1}=E_0^s\\&\varphi''_{s,2}=E_0^s+E_1^s*\left(\tfrac{1}{2}\right)+E_2^s*\left(\tfrac{1}{2}\right)^2\\&\varphi''_{s,3}=E_0^s+E_1^s*(1)+E_2^s*(1)^2\end{aligned} \quad [A27]$$

$$\begin{aligned}\psi'_{s,1} &= Q_0^s \\ \psi'_{s,2} &= Q_0^s + Q_1^s * \left(\tfrac{1}{2}\right) + Q_2^s * \left(\tfrac{1}{2}\right)^2 \\ \psi'_{s,3} &= Q_0^s + Q_1^s * (1) + Q_2^s * (1)^2\end{aligned} \quad [A28]$$

$$\begin{aligned}\psi''_{s,1} &= R_0^s \\ \psi''_{s,2} &= R_0^s + R_1^s * \left(\tfrac{1}{2}\right) + R_2^s * \left(\tfrac{1}{2}\right)^2 \\ \psi''_{s,3} &= R_0^s + R_1^s * (1) + R_2^s * (1)^2\end{aligned} \quad [A29]$$

$$\begin{aligned}-\varepsilon_s \left(c''_{s,2}\right)\omega &= \tfrac{1}{l_s}\left[\tfrac{D_{\text{eff,s}}}{l_s}\left(2A_2^s\right)\right] \\ \varepsilon_s \left(c'_{s,2}\right)\omega &= \tfrac{1}{l_s}\left[\tfrac{D_{\text{eff,s}}}{l_s}\left(2B_2^s\right)\right]\end{aligned} \quad [A30]$$

$$\begin{aligned}-\tfrac{1}{l_s}\left[\tfrac{\kappa_{\text{eff,s}}}{l_s}\left(2Q_2^s\right)\right] + \tfrac{1}{l_s}\left[\tfrac{2\kappa_{\text{eff,s}}RT}{Fc_0}\tfrac{(1-t_+)}{l_s}\left(2A_2^s\right)\right] &= 0 \\ -\tfrac{1}{l_s}\left[\tfrac{\kappa_{\text{eff,s}}}{l_s}\left(2R_2^s\right)\right] + \tfrac{1}{l_s}\left[\tfrac{2\kappa_{\text{eff,s}}RT}{Fc_0}\tfrac{(1-t_+)}{l_s}\left(2B_2^s\right)\right] &= 0\end{aligned} \quad [A31]$$

The boundary conditions at the anode-separator interface lead to:

$$\begin{aligned}c'_{n,3} &= c'_{s,1} \\ c''_{n,3} &= c''_{s,1} \\ \psi'_{n,3} &= \psi'_{s,1} \\ \psi''_{n,3} &= \psi''_{s,1}\end{aligned} \quad [A32]$$

And the boundary conditions at the separator-cathode interface lead to:

$$\begin{aligned}c'_{s,3} &= c'_{p,1} \\ c''_{s,3} &= c''_{p,1} \\ \psi'_{s,3} &= \psi'_{p,1} \\ \psi''_{s,3} &= \psi''_{p,1}\end{aligned} \quad [A33]$$

Equations in the positive electrode.—Again, a similar treatment in the positive electrode leads to the following set of equations.

$$\begin{aligned}c'_{p,1} &= A_0^p \\ c'_{p,2} &= A_0^p + A_1^p * \left(\tfrac{1}{2}\right) + A_2^p * \left(\tfrac{1}{2}\right)^2 \\ c'_{p,3} &= A_0^p + A_1^p * (1) + A_2^p * (1)^2\end{aligned} \quad [A34]$$

$$\begin{aligned}c''_{p,1} &= B_0^p \\ c''_{p,2} &= B_0^p + B_1^p * \left(\tfrac{1}{2}\right) + B_2^p * \left(\tfrac{1}{2}\right)^2 \\ c''_{p,3} &= B_0^p + B_1^p * (1) + B_2^p * (1)^2\end{aligned} \quad [A35]$$

$$\begin{aligned}\varphi'_{p,1} &= C_0^p \\ \varphi'_{p,2} &= C_0^p + C_1^p * \left(\tfrac{1}{2}\right) + C_2^p * \left(\tfrac{1}{2}\right)^2 \\ \varphi'_{p,3} &= C_0^p + C_1^p * (1) + C_2^p * (1)^2\end{aligned} \quad [A36]$$

$$\begin{aligned}\varphi''_{p,1} &= E_0^p \\ \varphi''_{p,2} &= E_0^p + E_1^p * \left(\tfrac{1}{2}\right) + E_2^p * \left(\tfrac{1}{2}\right)^2 \\ \varphi''_{p,3} &= E_0^p + E_1^p * (1) + E_2^p * (1)^2\end{aligned} \quad [A37]$$

$$\begin{aligned}\psi'_{p,1} &= Q_0^p \\ \psi'_{p,2} &= Q_0^p + Q_1^p * \left(\tfrac{1}{2}\right) + Q_2^p * \left(\tfrac{1}{2}\right)^2 \\ \psi'_{p,3} &= Q_0^p + Q_1^p * (1) + Q_2^p * (1)^2\end{aligned} \quad [A38]$$

$$\begin{aligned}\psi''_{p,1} &= R_0^p \\ \psi''_{p,2} &= R_0^p + R_1^p * \left(\tfrac{1}{2}\right) + R_2^p * \left(\tfrac{1}{2}\right)^2 \\ \psi''_{p,3} &= R_0^p + R_1^p * (1) + R_2^p * (1)^2\end{aligned} \quad [A39]$$

The governing equations in the positive electrode at the collocation point are given by:

$$\begin{aligned}-\varepsilon_p \left(c''_{p,2}\right)\omega = \tfrac{1}{l_p}\left[\tfrac{D_{\text{eff,p}}}{l_p}\left(2A_2^p\right)\right] + a_p(1-t_+)\Bigg(\tfrac{i0_p(\alpha_A+\alpha_C)}{RT}\left(\left(\varphi'_{p,2}\right) - \left(\psi'_{p,2}\right)\right. \\ \left. - dUdC_p * cps'\right) - \tfrac{\omega C dl_p}{F}\left(\left(\varphi''_{p,2}\right) - \left(\psi''_{p,2}\right)\right)\Bigg)\end{aligned} \quad [A40]$$

$$\begin{aligned}\varepsilon_p \left(c'_{p,2}\right)\omega = \tfrac{1}{l_p}\left[\tfrac{D_{\text{eff,p}}}{l_p}\left(2B_2^p\right)\right] + a_p(1-t_+)\Bigg(\tfrac{i0_p(\alpha_A+\alpha_C)}{RT}\left(\left(\varphi''_{p,2}\right) - \left(\psi''_{p,2}\right)\right. \\ \left. - dUdC_p * cps''\right) + \tfrac{\omega C dl_p}{F}\left(\left(\varphi'_{p,2}\right) - \left(\psi'_{p,2}\right)\right)\Bigg)\end{aligned}$$

$$\begin{aligned}\tfrac{1}{l_p}\left[\tfrac{-\sigma_{\text{eff,p}}}{l_p}\left(2C_2^p\right)\right] - \tfrac{1}{l_p}\left[\tfrac{\kappa_{\text{eff,p}}}{l_p}\left(2Q_2^p\right)\right] + \tfrac{1}{l_p}\left[\tfrac{2\kappa_{\text{eff,p}}RT}{Fc_0}\tfrac{(1-t_+)}{l_p}\left(2A_2^p\right)\right] &= 0 \\ \tfrac{1}{l_p}\left[\tfrac{-\sigma_{\text{eff,p}}}{l_p}\left(2E_2^p\right)\right] - \tfrac{1}{l_p}\left[\tfrac{\kappa_{\text{eff,p}}}{l_p}\left(2R_2^p\right)\right] + \tfrac{1}{l_p}\left[\tfrac{2\kappa_{\text{eff,p}}RT}{Fc_0}\tfrac{(1-t_+)}{l_p}\left(2B_2^p\right)\right] &= 0\end{aligned} \quad [A41]$$

$$\begin{aligned}\tfrac{1}{l_p}\left[\tfrac{\sigma_{\text{eff,p}}}{l_p}\left(2C_2^p\right)\right] = a_p F\Bigg(\tfrac{i0_p(\alpha_A+\alpha_C)}{RT}\left(\left(\varphi'_{p,2}\right) - \left(\psi'_{p,2}\right) - dUdC_p * cps'\right) \\ - \tfrac{\omega C dl_p}{F}\left(\left(\varphi''_{p,2}\right) - \left(\psi''_{p,2}\right)\right)\Bigg)\end{aligned} \quad [A42]$$

$$\begin{aligned}\tfrac{1}{l_p}\left[\tfrac{\sigma_{\text{eff,p}}}{l_p}\left(2E_2^p\right)\right] = a_p F\Bigg(\tfrac{i0_p(\alpha_A+\alpha_C)}{RT}\left(\left(\varphi''_{p,2}\right) - \left(\psi''_{p,2}\right) - dUdC_p * cps''\right) \\ + \tfrac{\omega C dl_p}{F}\left(\left(\varphi'_{p,2}\right) - \left(\psi'_{p,2}\right)\right)\Bigg)\end{aligned}$$

Where cps' and cps'' are the real and imaginary parts of the surface concentrations of the particle in the solid-phase respectively in the positive electrode, and similar to the negative electrode, are given by the analytical solution of the solid-phase equations.

The additional boundary conditions at the separator-cathode interface are given by:

$$\begin{aligned}\tfrac{-D_{\text{eff,s}}}{l_s}\left(A_1^s + 2A_2^s(1)\right) &= \tfrac{-D_{\text{eff,p}}}{l_p}\left(A_1^p\right) \\ \tfrac{-D_{\text{eff,s}}}{l_s}\left(B_1^s + 2B_2^s(1)\right) &= \tfrac{-D_{\text{eff,p}}}{l_p}\left(B_1^p\right) \\ \tfrac{-\kappa_{\text{eff,s}}}{l_s}\left(Q_1^s + 2Q_2^s(1)\right) &= \tfrac{-\kappa_{\text{eff,p}}}{l_p}\left(Q_1^p\right) \\ \tfrac{-\kappa_{\text{eff,s}}}{l_s}\left(R_1^s + 2R_2^s(1)\right) &= \tfrac{-\kappa_{\text{eff,p}}}{l_p}\left(R_1^p\right) \\ \left(C_1^p\right) &= 0 \\ \left(E_1^p\right) &= 0\end{aligned} \quad [A43]$$

The remaining boundary conditions at the cathode current collector are given by:

$$\begin{aligned}\mathrm{A}_1^p + 2\mathrm{A}_2^p(1) &= 0 \\ \mathrm{B}_1^p + 2\mathrm{B}_2^p(1) &= 0 \\ \tfrac{1}{l_p}\left(Q_1^p + 2Q_2^p(1)\right) &= 0 \\ \tfrac{1}{l_p}\left(R_1^p + 2R_2^p(1)\right) &= 0 \\ \left(\tfrac{1}{l_p}\left(C_1^p + 2C_2^p(1)\right)\right) &= -\tfrac{I}{\sigma_{eff,p}} \\ \left(\tfrac{1}{l_p}\left(E_1^p + 2E_2^p(1)\right)\right) &= 0\end{aligned} \quad [A44]$$

The resulting set of Equations A1–A15 and A19–A44 can now be solved simultaneously to obtain all the unknowns of the system. The linear impedance of the battery is given by:

$$\begin{aligned}\mathrm{Re}\left(\bar{Z}\right) &= \left|\tfrac{\varphi'_{p,1} - \psi'_{n,N+2}}{I}\right| \\ \mathrm{Img}\left(\bar{Z}\right) &= \left|\tfrac{\varphi''_{p,1} - \psi''_{n,N+2}}{I}\right|\end{aligned} \quad [A45]$$

Analytical solution for solid-phase equations.—The dynamics of diffusion inside the solid particles for constant diffusivity is represented in the spherical coordinates by the equation:

$$\frac{\partial c_i^s}{\partial t} = \frac{1}{r^2}\frac{\partial}{\partial r}\left[r^2 D_i^s \frac{\partial c_i^{s\prime}}{\partial r}\right] \quad [A46]$$

Applying Fourier transform, the following equations can be derived for the respective real and imaginary parts:

$$\begin{aligned}-\omega c_i^{s\prime\prime} &= \tfrac{1}{r^2}\tfrac{\partial}{\partial r}\left[r^2 D_i^s \tfrac{\partial c_i^{s\prime}}{\partial r}\right] \\ \omega c_i^{s\prime} &= \tfrac{1}{r^2}\tfrac{\partial}{\partial r}\left[r^2 D_i^s \tfrac{\partial c_i^{s\prime\prime}}{\partial r}\right]\end{aligned} \quad [A47]$$

With the corresponding boundary conditions given by:

$$\left.\frac{\partial c_i^{s\prime}}{\partial r}\right|_{r=0} = 0$$
$$\left.\frac{\partial c_i^{s\prime\prime}}{\partial r}\right|_{r=0} = 0$$
$$-D_i^s \left.\frac{\partial c_i^{s\prime}}{\partial r}\right|_{r=R_i} = j'_i$$
$$-D_i^s \left.\frac{\partial c_i^{s\prime\prime}}{\partial r}\right|_{r=R_i} = j''_i \quad [A48]$$

The following equation can be derived using a simple variable transformation as shown:

$$-w^2 cim(Y) = \frac{d^2}{dY^2} cre(Y)$$
$$w^2 cre(Y) = \frac{d^2}{dY^2} cim(Y) \quad [A49]$$

Where the new variables are given by the relations:

$$Y = \frac{r}{R_i}$$
$$cre(Y) = Y \cdot c_i^{s\prime}(r)$$
$$cim(Y) = Y \cdot c_i^{s\prime\prime}(r) \quad [A50]$$
$$w = \sqrt{\frac{\omega R_i^2}{D_i^s}}$$

The boundary conditions for the transformed variables $cre(Y)$ and $cim(Y)$ at $Y = 0$ are given by:

$$cre(Y)|_{Y=0} = 0 \cdot c_i^{s\prime}(r) = 0$$
$$cim(Y)|_{Y=0} = 0$$
$$\left.\frac{d\, cre(Y)|}{dY}\right|_{Y=0} = \beta \quad [A51]$$
$$\left.\frac{d\, cim(Y)|}{dY}\right|_{Y=0} = \delta$$

Where β and δ are unknowns to be determined.

The analytical solution for Equations A49 and boundary conditions A51 is given by:

$$cre(Y) = \frac{\sqrt{2}\left(\cosh\left(1/2\sqrt{2}wY\right)\sin\left(1/2\sqrt{2}wY\right)\beta - \cosh\left(1/2\sqrt{2}wY\right)\sin\left(1/2\sqrt{2}wY\right)\delta + \sinh\left(1/2\sqrt{2}wY\right)\cos\left(1/2\sqrt{2}wY\right)\beta + \sinh\left(1/2\sqrt{2}wY\right)\cos\left(1/2\sqrt{2}wY\right)\delta\right)}{2w} \quad [A52]$$
$$cim(Y) = \frac{\sqrt{2}\left(\cosh\left(1/2\sqrt{2}wY\right)\sin\left(1/2\sqrt{2}wY\right)\beta + \cosh\left(1/2\sqrt{2}wY\right)\sin\left(1/2\sqrt{2}wY\right)\delta - \sinh\left(1/2\sqrt{2}wY\right)\cos\left(1/2\sqrt{2}wY\right)\beta + \sinh\left(1/2\sqrt{2}wY\right)\cos\left(1/2\sqrt{2}wY\right)\delta\right)}{2w}$$

This relation can be used to obtain the original variables as:

$$c_i^{s\prime}(r) = \frac{cre(Y)}{Y} = \frac{\sqrt{2}\left(\cosh\left(1/2\sqrt{2}wY\right)\sin\left(1/2\sqrt{2}wY\right)\beta - \cosh\left(1/2\sqrt{2}wY\right)\sin\left(1/2\sqrt{2}wY\right)\delta + \sinh\left(1/2\sqrt{2}wY\right)\cos\left(1/2\sqrt{2}wY\right)\beta + \sinh\left(1/2\sqrt{2}wY\right)\cos\left(1/2\sqrt{2}wY\right)\delta\right)}{2wY} \quad [A53]$$
$$c_i^{s\prime\prime}(r) = \frac{cim(Y)}{Y} = \frac{\sqrt{2}\left(\cosh\left(1/2\sqrt{2}wY\right)\sin\left(1/2\sqrt{2}wY\right)\beta + \cosh\left(1/2\sqrt{2}wY\right)\sin\left(1/2\sqrt{2}wY\right)\delta - \sinh\left(1/2\sqrt{2}wY\right)\cos\left(1/2\sqrt{2}wY\right)\beta + \sinh\left(1/2\sqrt{2}wY\right)\cos\left(1/2\sqrt{2}wY\right)\delta\right)}{2wY}$$

The real and imaginary parts of the surface concentration of the particle is defined as:

$$cis' = c_i^{s\prime}(r)|_{r=R_i} = \left.\frac{cre(Y)}{Y}\right|_{Y=1} = \frac{\sqrt{2}\left(\cosh\left(1/2\sqrt{2}w\right)\sin\left(1/2\sqrt{2}w\right)\beta - \cosh\left(1/2\sqrt{2}w\right)\sin\left(1/2\sqrt{2}w\right)\delta + \sinh\left(1/2\sqrt{2}w\right)\cos\left(1/2\sqrt{2}w\right)\beta + \sinh\left(1/2\sqrt{2}w\right)\cos\left(1/2\sqrt{2}w\right)\delta\right)}{2w} \quad [A54]$$
$$cis'' = c_i^{s\prime\prime}(r)|_{r=R_i} = \left.\frac{cim(Y)}{Y}\right|_{Y=1} = \frac{\sqrt{2}\left(\cosh\left(1/2\sqrt{2}w\right)\sin\left(1/2\sqrt{2}w\right)\beta + \cosh\left(1/2\sqrt{2}w\right)\sin\left(1/2\sqrt{2}w\right)\delta - \sinh\left(1/2\sqrt{2}w\right)\cos\left(1/2\sqrt{2}w\right)\beta + \sinh\left(1/2\sqrt{2}w\right)\cos\left(1/2\sqrt{2}w\right)\delta\right)}{2w}$$

The boundary conditions at $r = R_i$ contains $j_i'$and j_i'', which are functions of $cis'$and cis''respectively. Same conditions are used to obtain the unknown variables β and δ. From Table AII, after substituting the expressions for j_i', j_i'', η_i' and η_i'', the boundary conditions can be rewritten as:

$$\left.\frac{\partial c_i^{s\prime}}{\partial r}\right|_{r=R_i} = -\frac{j'_i}{D_i^s} = A_1 + B_1(cis')$$
$$\left.\frac{\partial c_i^{s\prime\prime}}{\partial r}\right|_{r=R_i} = -\frac{j''_i}{D_i^s} = A_2 + B_2(cis'') \quad [A55]$$

Where A_1, B_1, A_2 *and* B_2 are given by:

$$A_1 = -\frac{i0_i R_i(\alpha_a+\alpha_c)\left(\Phi'_{1,i} - \Phi'_{2,i}\right)}{RTD_i^s}$$
$$B_1 = \frac{i0_i R_i(\alpha_a+\alpha_c)dUdC_i}{RTD_i^s}$$
$$A_2 = -\frac{i0_i R_i(\alpha_a+\alpha_c)\left(\Phi''_{1,i} - \Phi''_{2,i}\right)}{RTD_i^s} \quad [A56]$$
$$B_2 = \frac{i0_i R_i(\alpha_a+\alpha_c)dUdC_i}{RTD_i^s}$$

Equation A53 is used to calculate the slope of $c_i^{s\prime}$ and $c_i^{s\prime\prime}$ required in Equation A55, which is then solved simultaneously with Equation A54 to get the required unknowns β and δ. The last step is too complicated to be written here, but can be performed using a symbolic mathematical tool, such as *Mathematica* or *Maple*. Once β and δ are known, Equation A54 can be used to calculate the surface concentration, and the effect of the pseudo radial coordinate can be decoupled.

List of Symbols

$c_i{}'$	Real part of the electrolyte concentration in region 'i', $i = \{p, s, n\}$
$c_i{}''$	Imaginary part of the electrolyte concentration in region 'i', $i = \{p, s, n\}$
$c_i^{s\prime}$	Real part of the solid-phase concentration in region 'i', $i = \{p, n\}$
$c_i^{s\prime\prime}$	Imaginary part of the solid-phase concentration in region 'i', $i = \{p, n\}$
cps'	Real part of the solid-phase concentration at the surface of the particle in the positive electrode
cps''	Imaginary part of the solid-phase concentration at the surface of the particle in the positive electrode
cns'	Real part of the solid-phase concentration at the surface of the particle in the negative electrode
cns''	Imaginary part of the solid-phase concentration at the surface of the particle in the negative electrode
j_i'	Real part of the pore-wall flux in region 'i', $i = \{p, n\}$
j_i''	Imaginary part of the pore-wall flux in region 'i', $i = \{p, n\}$
$j'_{dl,i}$	Real part of the double-layer flux in region 'i', $i = \{p, n\}$
$j''_{dl,i}$	Imaginary part of the double-layer flux in region 'i', $i = \{p, n\}$
X	Scaled x-coordinate

Greek

$\Phi'_{1,i}$	Real part of the solid-phase potential in region 'i', $i = \{p, n\}$
$\Phi''_{1,i}$	Imaginary part of the solid-phase potential in region 'i', $i = \{p, n\}$
$\Phi'_{2,i}$	Real part of the electrolyte-phase potential in region 'i', $i = \{p, s, n\}$
$\Phi''_{2,i}$	Imaginary part of the electrolyte-phase potential in region 'i', $i = \{p, s, n\}$
η_i'	Real part of the overpotential in region 'i', $i = \{p, n\}$
η_i''	Imaginary part of the overpotential in region 'i', $i = \{p, n\}$

Subscripts

eff	Effective, as for diffusivity or conductivity
c	Related to electrolyte concentration
c^s	Related to solid-phase concentration
n	Related to the negative electrode—the anode
p	Related to the positive electrode—the cathode
s	Related to the separator
dl	Related to the double-layer

Superscripts

avg	Average, as for solid-phase concentration
$surf$	Surface, as for solid-phase concentration
s	Related to solid phase
1	Related to the solid-phase potential
2	Related to the liquid-phase potential
$'$	Representing the real part
$''$	Representing the imaginary part

ORCID

Matthew D. Murbach https://orcid.org/0000-0002-6583-5995
Yanbo Qi https://orcid.org/0000-0001-5852-6011
Venkat R. Subramanian https://orcid.org/0000-0002-2092-9744

References

1. M. E. Orazem and B. Tribollet, *Electrochemical Impedance Spectroscopy*, Wiley, New Jersey (2008).
2. G. Barsoukov and J. R. Macdonald, *Impedance Spectroscopy: Theory, Experiment, and Applications*, Wiley-Interscience, New Jersey (2005).
3. M. G. S. R. Thomas, P. G. Bruce, and J. B. Goodenough, *Journal of the Electrochemical Society*, **132**, 1521 (1985).
4. P. Yu, B. N. Popov, J. A. Ritter, and R. E. White, *Journal of the Electrochemical Society*, **146**, 8 (1999).
5. M. Dubarry, A. Devie, and B. Y. Liaw, *Journal of Energy and Power Sources*, **1**, 242 (2014).
6. M. Dubarry, C. Truchot, and B. Y. Liaw, *Journal of Power Sources*, **219**, 204 (2012).
7. C. Pastor-Fernandez, K. Uddin, G. H. Chouchelamane, W. D. Widanage, and J. Marco, *Journal of Power Sources*, **360**, 301 (2017).
8. U. Tröltzsch, O. Kanoun, and H. R. Tränkler, *Electrochimica Acta*, **51**, 1664 (2006).
9. S. Fletcher, *Journal of the Electrochemical Society*, **141**, 1823 (1994).
10. V. Ramadesigan, P. W. C. Northrop, S. De, S. Santhanagopalan, R. D. Braatz, and V. R. Subramanian, *Journal of the Electrochemical Society*, **159**, R31 (2012).
11. M. Doyle, J. P. Meyers, and J. Newman, *Journal of the Electrochemical Society*, **147**, 99 (2000).
12. R. Pollard and T. Comte, *Journal of The Electrochemical Society*, **136**, 3734 (1989).
13. M. D. Murbach and D. T. Schwartz, *Journal of the Electrochemical Society*, **164**, E3311 (2017).
14. D. W. Dees, K. G. Gallagher, D. P. Abraham, and A. N. Jansen, *Journal of the Electrochemical Society*, **160**, A478 (2013).
15. N. R. Amundson, *Mathematical methods in chemical engineering: matrices and their application*, Prentice-Hall, Englewood Cliffs, N. J (1966).
16. V. R. Subramanian, B. S. Haran, and R. E. White, *Computers & chemical engineering*, **23**, 287 (1999).
17. V. R. Subramanian and R. E. White, *Chemical engineering science*, **59**, 781 (2004).
18. J. C. Forman, S. Bashash, J. L. Stein, and H. K. Fathy, *Journal of the Electrochemical Society*, **158**, A93 (2011).
19. J. C. Forman, S. J. Moura, J. L. Stein, and H. K. Fathy, *Journal of Power Sources*, **210**, 263 (2012).
20. L. Cai and R. E. White, *Journal of Power Sources*, **217**, 248 (2012).
21. L. Cai and R. E. White, *Journal of the Electrochemical Society*, **156**, A154 (2009).
22. S. Lee, Y. Kim, and H. Chun, *Electrochimica Acta*, **47**, 1055 (2002).
23. P. W. C. Northrop, V. Ramadesigan, S. De, and V. R. Subramanian, *Journal of the Electrochemical Society*, **158**, A1461 (2011).
24. V. Ramadesigan, V. Boovaragavan, J. C. Pirkle, and V. R. Subramanian, *Journal of The Electrochemical Society*, **157**, A854 (2010).
25. C. Y. Wang, W. B. Gu, and B. Y. Liaw, *Journal of the Electrochemical Society*, **145**, 3407 (1998).
26. Q. Zhang and R. E. White, *Journal of Power Sources*, **165**, 880 (2007).
27. S. Liu, *Solid State Ionics*, **177**, 53 (2006).
28. J. P. Meyers, M. Doyle, R. M. Darling, and J. Newman, *Journal of the Electrochemical Society*, **147**, 2930 (2000).
29. S. Devan, V. R. Subramanian, and R. E. White, *Journal of the Electrochemical Society*, **151**, A905 (2004).
30. P. M. Gomadam, J. W. Weidner, T. A. Zawodzinski, and A. P. Saab, *Journal of the Electrochemical Society*, **150**, E371 (2003).
31. V. R. Subramanian, V. Boovaragavan, K. Potukuchi, V. D. Diwakar, and A. Guduru, *Electrochem. Solid-State Lett.*, **10**, A25 (2007).
32. G. Sikha and R. E. White, *Journal of the Electrochemical Society*, **155**, A893 (2008).
33. G. Sikha and R. E. White, *Journal of the Electrochemical Society*, **154**, A43 (2007).
34. J. Huang and J. Zhang, *Journal of the Electrochemical Society*, **163**, A1983 (2016).
35. Comsol Multiphysics, www.comsol.com, last accessed June 15th, 2017.
36. J. Villadsen and M. L. Michelsen, *Solution of Differential Equation Models by Polynomial Approximation*, Prentice-Hall, Inc., Englewood Cliffs, NJ (1978).
37. B. A. Finlayson, *Nonlinear Analysis in Chemical Engineering*, McGraw-Hill, New York (1980).
38. S. K. Gupta, *Numerical Methods for Engineers*, New Age International (P) Ltd., Publishers, Delhi (2010).
39. E. Hairer and G. Wanner, *Solving ordinary differential equations II: Stiff and differential-algebraic problems*, Springer-Verlag, Berlin (1996).
40. C. Liu, Z. G. Neale, and G. Cao, *Materials Today*, **19**, 109 (2016).
41. N. Nitta and G. Yushin, *Particle & Particle Systems Characterization*, **31**, 317 (2014).
42. M. Doyle and J. Newman, *Electrochimica Acta*, **40**, 2191 (1995).
43. P. Arora, M. Doyle, A. S. Gozdz, R. E. White, and J. Newman, *Journal of Power Sources*, **88**, 219 (2000).